Subject Category: Protein structure and analysis

Small conformational changes in IgG1 detected as acidic charge variants by cation exchange chromatography

Masakazu Fukuda[a,b,*] · Melissa A. Graewert[c] · Cy M. Jeffries[c] · Dmitri I. Svergun[c] · Tadao Yamazaki[a] · Akiko Koga[a] · Yuji Yamanaka[a]

[a] *Production Engineering Department, Chugai Pharmaceutical Co., Ltd.,*
5-5-1 Ukima, Kita-ku, Tokyo 115-8543, Japan

[b] *Laboratory of Functional Molecular Chemistry, Kobe Pharmaceutical University,*
4-19-1, Motoyamakita-machi, Higashinada-ku, Kobe 658-8558, Japan

[c] *European Molecular Biology Laboratory (EMBL) Hamburg Unit, c/o Deutsches Elektronen Synchrotron (DESY), 22607 Hamburg, Germany*

[*] Corresponding author.
E-mail address: fukudamk@kobepharma-u.ac.jp (M. Fukuda).

ABSTRACT

Fully characterizing the post-translational modifications present in charge variants of therapeutic monoclonal antibodies (mAbs), particularly acidic variants, is challenging and remains an open area of investigation. In this study, to test the possibility that chromatographically separated acidic fractions of therapeutic mAbs contain conformational variants, we undertook a mAb refolding approach using as a case study an IgG1 that contains many unidentified acidic peaks with few post-translational modifications, and examined whether different acidic peak fractions could be generated corresponding to these variants. The IgG1 drug substance was denatured by guanidine hydrochloride, without a reducing agent present, and gradually refolded by stepwise dialysis against arginine hydrochloride used as an aggregation suppressor. Each acidic chromatographic peak originally contained in the IgG1 drug substance was markedly increased by this stepwise refolding process, indicating that these acidic variants are conformational variants. However, no conformational changes were detected by small-angle X-ray scattering experiments for the whole IgG1, indicating that the conformational changes are minor. Chromatographic, thermal and fluorescence analyses suggested that the conformational changes are a localized denaturation effect centred around the aromatic amino acid regions. This study provides new insights into the characterization of acidic variants that are currently not fully understood.

Keywords:

Acidic variant

Cation-exchange chromatography

Conformational change

Monoclonal antibody

Refolding

Abbreviations

ANS	1-Anilino-8-naphthalene sulfonate
CEX	Cation-exchange chromatography
DSF	Differential scanning fluorimetry
DS	Drug substance
DLS	Dynamic light scattering
R_h	Hydrodynamic radius
HIC	Hydrophobic interaction chromatography
D_{max}	Maximum dimension
λ_{max}	Maximum emission wavelength
$p(r)$	Pair–distance distribution function
R_g	Radius of gyration
SEC	Size-exclusion chromatography
SAXS	Small-angle X-ray scattering
T_m	Thermal denaturation temperature

1. Introduction

Therapeutic monoclonal antibodies (mAbs), like other proteins, are susceptible to chemical and enzymatic post-translational modifications during their manufacture, resulting in a heterogeneous mix of variants containing various post-translational modifications [1]. One of the most common forms of heterogeneity is charge variation, and thorough characterization of charge variants is important in order to identify critical quality attributes. Ion-exchange chromatography is the gold standard method for charge variant analysis. Cation-exchange chromatography (CEX) is the default method because many therapeutic mAbs have basic isoelectric points [2]. Isoelectric focusing is also employed, where the separation is based on the net charge of the protein. However, isoelectric focusing is less sensitive to the localized charge distribution on the protein surface. Charge variants with the same isoelectric point by isoelectric focusing have been reported to show multiple peaks when analyzed by chromatographic techniques [3–5], suggesting that net charge is not the only factor affecting the chromatographic behavior, and that localized charge distribution and stereochemistry may alter the chromatographic elution profiles in subtle ways [6].

Charge variants are classified as either acidic or basic relative to the main variant. Acidic variants exhibit an isoelectric point lower than that of the main variant and elute earlier than the main peak when analyzed by CEX, whereas basic variants exhibit a higher isoelectric point and elute later. Various post-translational modifications have been reported to contribute to the formation of acidic and basic variants [6–9]. Post-translational modifications that can lead to the formation of acidic variants include sialylation, asparagine deamidation, glycation, and C-terminal lysine cleavage. Factors that can lead to the formation of basic variants include the presence of C-terminal lysine, N-terminal glutamine, C-terminal amidation, isomerization, and succinimide formation. Some post-translational modifications directly alter the net charge of the proteins while others induce conformational changes that affect the local charge distribution. Interestingly, Ponniah et al. reported succinimide species eluting as acidic variants in anion-exchange chromatography [10], contrary to previous reports of succinimide species being classified as basic variants [11–13]. A difference in net charge cannot explain the elution of succinimide species as acidic variants, and the authors of that report suggested that succinimide formation causes a conformational change, which leads to differences in surface charge distribution.

Although several types of post-translational modification have already been identified in various mAbs, the full characterization of post-translational modifications in charge variants of mAbs, particularly acidic variants, is challenging and remains an open area of investigation [9, 14–16]. It is usually found that the sum of the quantitative values of the identified acidic species does not fully account for the total acidic regions in the elution profile. We previously characterized acidic variants of an IgG1 mAb internally by using standard techniques, but we could hardly detect differences between the main peak fraction and the acidic peak fractions (unpublished results). Briefly, sialidase digestion partially decreased the area of the most prevalent acidic peak and increased the area of the main peak, indicating that the acidic peak is only partially composed of IgG1 containing terminal sialic acid on the Fc N-glycans. Glycation was not identified as a main attribute because the decrease in the peak areas of the acidic fractions by enzymatic deglycosylation with PNGase F was limited to the effect of sialylation. The deglycosylated main and acidic fractions were reduced and carboxymethylated, and then the molecular weights of their heavy and light chains were determined by liquid chromatography-mass spectrometry. As a result, the two molecular weights were found to be completely identical between the main and acidic fractions. Furthermore, trypsin peptide mapping of the deglycosylated main and acidic fractions revealed that the acidic variants do not include primary sequence modifications (such as deamidation). The most probable cause of this gap may be slight conformational differences that are difficult to detect. Interestingly, Gervais et al. report that, based on results of extended characterization and refolding studies, the most prevalent acidic peak of *Erwinia chrysanthemi* L-asparaginase (a 140-kDa homotetramer in its active form) is a conformational variant with no primary sequence modifications [17].

In this study, to test the possibility that the acidic fractions of therapeutic mAbs contain conformational variants, we examined whether additional acidic peaks could be generated by a refolding process without a reducing agent, using as an example the aforementioned IgG1 mAb that contains many unidentified acidic peaks with few post-translational modifications. Since acidic peaks were generated by the refolding process, we considered these acidic peaks as conformational variants and examined the conformational changes that occur in the acidic fraction using various analytical methods.

2. Materials and methods

2.1 Materials

The drug substance (DS) used in this study was a humanized IgG1 mAb to human interleukin-6 receptor, manufactured by Chugai Pharmaceutical (Tokyo, Japan). The theoretical isoelectric point of the IgG1 was 9.3. Cytochrome C from equine heart and ribonuclease A from bovine pancreas were purchased from Merck (Darmstadt, Germany). 2-Morpholinoethanesulfonic acid monohydrate (MES) was purchased from Dojindo Laboratories (Kumamoto, Japan). 1-Anilino-8-naphthalene sulfonate (ANS) was purchased from Cayman Chemical (Ann Arbor, MI, USA). All other chemicals were purchased from Fujifilm Wako Pure Chemical Corporation (Osaka, Japan). The protein samples were formulated in a buffer of 25 mM MES/NaOH, 150 mM NaCl, pH 6.1, unless otherwise noted. The protein concentration was determined using UV absorbance at 280 nm.

2.2 Protein refolding by stepwise dialysis

The IgG1 DS, cytochrome C and ribonuclease A, as well as the main and acidic peak fractions isolated from the IgG1 DS by preparative CEX described below were used in refolding studies without a reducing agent, where all unfolding/refolding steps were maintained at pH 6.1 and performed at room temperature (nominally 23°C). The protein samples were unfolded in the MES formulation buffer in the presence of 6 M guanidine hydrochloride at a protein concentration of 0.1 mg/mL for 1 hour. The guanidine hydrochloride was gradually removed to refold the protein by stepwise dialysis using a Slide-A-Lyzer dialysis cassette (20,000 MWCO for IgG1 samples; 3,500 MWCO for cytochrome C and ribonuclease A samples; Thermo Fisher Scientific, Waltham, MA, USA) against 100-fold volume excess of MES formulation buffer with 0.5 M arginine hydrochloride in combination with systematically decreasing concentrations of guanidine hydrochloride (i.e., 3 M, 2 M, 1 M, and 0.5 M) for more than 6 hours each, followed by a final dialysis step against the MES formulation buffer without arginine hydrochloride or guanidine hydrochloride for more than 18 hours.

2.3 Cation-exchange chromatography (CEX)

The main and acidic mAb peak fractions were isolated from the IgG1 DS by preparative CEX, using a Dionex UltiMate 3000 HPLC system (Thermo Fisher Scientific) equipped with a semi-preparative column,

Propac WCX-10 (9.0×250 mm, 10 μm, Thermo Fisher Scientific). Mobile phase A consisted of 25 mM MES/NaOH, pH 6.1 while mobile phase B was 25 mM MES/NaOH, 250 mM NaCl, pH 6.1. The IgG1 DS was diluted with mobile phase A and injected onto the column at a concentration of 22.5 mg/mL. The injection volume was 160 μL, where the column flow-rate was maintained at 1 mL/min throughout the ion exchange, and performed at 40°C. After sample injection, the column was run for 5 minutes using a mobile phase ratio of 63% v/v A and 37% v/v B followed by a linear elution gradient of 0.4% v/v mobile phase B per minute, ending at 50 minutes. The column was then washed for 10 minutes with 100% B. The protein elution was monitored by UV absorbance at 280 nm. Each collected sample was buffer-exchanged into the standard formulation buffer of 25 mM MES/NaOH, 150 mM NaCl, pH 6.1 and concentrated to over 3 mg/mL using Amicon Ultra filters (50,000 MWCO; Merck).

The elution profiles of IgG1, cytochrome C, and ribonuclease A samples were analyzed by analytical CEX, using an Agilent 1290 Infinity HPLC system (Santa Clara, CA, USA) equipped with an analytical weak cation exchange column, ProPac WCX-10 (4.0×250 mm, 10 μm, Thermo Fisher Scientific). Except as described below, the methods were the same as those for preparative CEX. Before chromatographic analysis, the protein samples were buffer-exchanged into mobile phase A and concentrated as needed by centrifugation using Amicon Ultra filters (50,000 MWCO for IgG1 samples, 3000 MWCO for cytochrome C and ribonuclease A samples; Merck). The protein samples were injected at a concentration of 0.5 mg/mL. The injection volumes were 30 μL for the IgG1 samples and 100 μL for cytochrome C and ribonuclease A, maintaining a flow rate of 0.5 mL/min at room temperature. For the IgG1 samples, after running the column for 5 minutes with 63% v/v A and 37% v/v B, a linear elution gradient of 0.4% v/v mobile phase B per minute was applied out to 80 minutes. For cytochrome C, a linear elution gradient of 0.4% v/v B per minute was applied after running the column at 46% v/v A and 54% v/v B for 5 minutes, ending at 55 minutes. For ribonuclease A, a linear elution gradient of 0.2% v/v B per minute was used after running the column at 67% v/v A and 33% v/v B for 5 minutes, for a total of 100 minutes (in this case, mobile phase B consisted of 25 mM MES/NaOH, 500 mM NaCl, pH 6.1). In all instances, and at the completion of the CEX gradient, the column was washed for 5 minutes with 100% v/v of the respective mobile phase B.

2.4 Size-exclusion chromatography (SEC)

The elution profiles of IgG1 samples were analyzed by SEC at room temperature, using an Agilent 1290 Infinity HPLC system equipped with a size exclusion column, TSK-gel G3000SW$_{XL}$ (7.8×300 mm, 5 μm, Tosoh, Tokyo, Japan). The IgG1 samples were injected at a concentration of 1 mg/mL, with an injection volume of 40 μL. A running buffer of 50 mM sodium phosphate, 300 mM NaCl, pH 7.0 was used at a flow rate of 0.5 mL/min. The protein elution was monitored by UV absorbance at 280 nm.

2.5 Hydrophobic interaction chromatography (HIC)

The elution profiles of the IgG1 samples were analyzed by HIC using an Agilent 1290 Infinity HPLC system equipped with a hydrophobic interaction column, ProPac HIC-10 (4.6×100 mm, 5 μm, Thermo Fisher Scientific). Before chromatographic analysis, the IgG1 samples were buffer-exchanged into a buffer of 25 mM MES/NaOH, pH 6.1 and concentrated as needed by centrifugation using Amicon Ultra filters (50,000 MWCO; Merck). The protein samples were injected at a concentration of 0.4 mg/mL. The injection volume was 10 μL. Mobile phase A was 100 mM sodium phosphate, pH 6.1. Mobile phase B was 100 mM sodium phosphate, 2 M $(NH_4)_2SO_4$, pH 6.1. The flow rate was set to 0.5 mL/min and the analysis was performed at room temperature. A linear elution gradient of 2% mobile phase A per minute was applied after running the column at 50% v/v A and 50% v/v B for 5 minutes, and ended at 20 minutes. The column was then washed for 10 minutes with 100% v/v A. The protein elution was monitored by UV absorbance at 280 nm.

2.6 Dynamic light scattering (DLS)

DLS measurements were performed using a DynaPro Plate Reader II (Wyatt Technology Corporation, Santa Barbara, CA, USA) to obtain the average hydrodynamic radius [R_h (nm)] at 25°C. The IgG1 samples were dispensed into a 384-well plate at a concentration of 0.5 mg/mL. The sample volume was 25 μL.

2.7 Small-angle X-ray scattering (SAXS)

SAXS experiments were performed at the EMBL P12 beam line (PETRA III, DESY synchrotron, Hamburg, Germany) [18]. An automated robotic sample changer (BioSAXS; Arinax, Grenoble, France) was employed to deliver the IgG1 samples (1 mg/mL) and corresponding matched buffers at 20°C under continuous flow to the beam line through a 1 mm capillary of the sample exposure unit [19]. Two-

dimensional SAXS patterns were collected using a PILATUS 6M pixel detector, a sample-detector distance of 3.0 m and a wavelength (λ) of 0.124 nm. A momentum transfer range of $0.026 < s < 7.288$ nm^{-1} (where $s = 4\pi\sin\theta/\lambda$, 2θ is the scattering angle) was covered. Data reduction were performed by the automated data pipeline SASFLOW [20]. Briefly, the isotropic two-dimensional scattering intensities were normalized to the intensity of the transmitted beam and azimuthally averaged to generate one-dimensional scattering profiles [$I(s)$ vs s]. Data collection was divided into 20 separate frames of 50 msec each. To exclude data from samples potentially affected by radiation damage, automated pairwise 1D data frame comparisons and subsequent data-frame rejection were employed, followed by undamaged sample frame averaging and buffer scattering subtraction. The radius of gyration (R_g) and extrapolated scattering to zero angle [$I(0)$] was obtained by employing the Guinier approximation [$\ln I(s)$ vs s for $sR_g < 1.3$] as well as the calculation of the scattering pair–distance distribution function [$p(r)$] from which the maximum dimension (D_{max}) was also estimated [21]. The fits to the theoretical scattering profile from the high-resolution crystal structure of a human IgG1 (pdb code:1hzh.pdb) were computed with CRYSOL [22].

2.8 Differential scanning fluorimetry (DSF)

DSF measurements were performed using a Prometheus NT.48 (NanoTemper Technologies, Munich, Germany) with UV transparent capillaries. In the DSF experiments, a buffer condition of 25 mM citrate/NaOH, 150 mM NaCl, pH 4.1 was used in addition to the standard formulation MES buffer at pH 6.1 because the thermal denaturation temperature (T_m) of the Fab domain at pH 6.1 exceeded this instrument's upper measurement temperature (i.e., 95°C). The IgG1 samples were buffer-exchanged into the buffer at pH 4.1 via centrifugation using Amicon Ultra filters (50,000 MWCO; Merck). The IgG1 samples were loaded into the capillaries at a concentration of 0.5 mg/mL. The loading volume was 11 μL. DSF scans were performed at a rate of 1°C/min from 15°C to 95°C. Thermal denaturation was measured by detecting the temperature-dependent changes in the ratio of intrinsic fluorescence at emission wavelengths of 330 and 350 nm (350 nm/330 nm). The T_m was determined from the peaks of the first derivative of the fluorescence ratio. Data were analyzed with ThermControl software (NanoTemper Technologies).

2.9 Fluorescence measurements

Fluorescence measurements were performed with a microplate spectrofluorometer Infinite M1000 (Tecan, Mannedorf, Switzerland). For the ANS fluorescence measurements, a concentrated stock solution of ANS (2 mM ANS in the standard formulation MES buffer) was added to each IgG1 sample (3 mg/mL) to obtain a final ANS concentration of 200 μM, and 20 μL of the mixed sample solution was dispensed into a 384-well black plate. Fluorescence spectra of ANS were recorded from 450 to 600 nm with an excitation wavelength of 385 nm at 25°C. The ANS fluorescence spectrum of each IgG1 sample was corrected by subtracting the spectrum of a blank solution of standard formulation MES buffer containing 200 μM ANS. For intrinsic fluorescence measurements, 20 μL of each IgG1 sample (3 mg/mL) was dispensed into a 384-well black plate. Intrinsic fluorescence spectra were recorded from 300 to 360 nm with an excitation wavelength of 285 nm at 25°C. The intrinsic fluorescence spectrum of each IgG1 sample was corrected by subtracting the spectrum of the blank solution of standard formulation MES buffer.

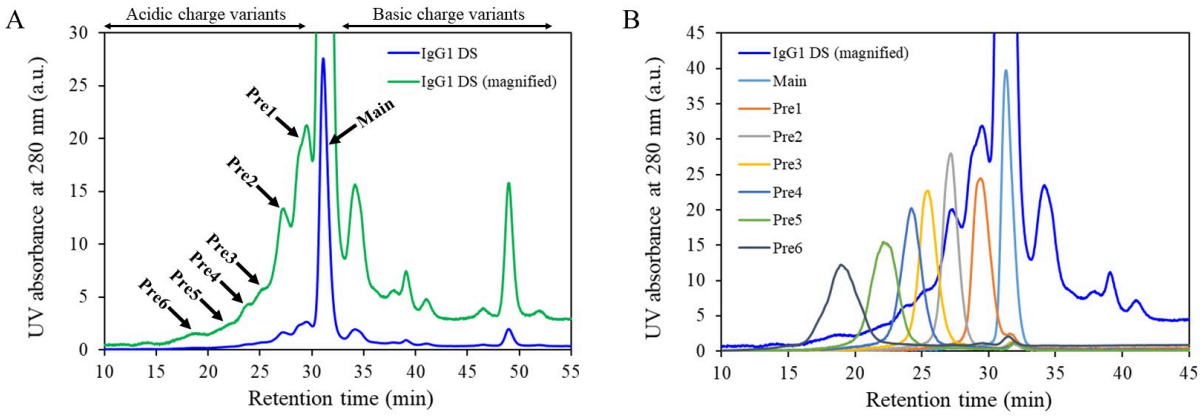

Fig. 1. (A) Representative CEX profile of the IgG1 drug substance (DS) used in this study. The acidic peaks investigated are designated *Pre1*, *Pre2*, *Pre3*, *Pre4*, *Pre5*, and *Pre6* in order of decreasing elution time. **(B)** CEX profiles of the *Main*, *Pre1*, *Pre2*, *Pre3*, *Pre4*, *Pre5*, and *Pre6* fractions isolated from the IgG1 DS. Magnified CEX profile of the IgG1 DS is shown as a reference.

3. Results

3.1 Purity check of isolated acidic and main fractions

A representative CEX profile of the IgG1 DS is shown in Figure 1A. A number of acidic/basic charge variants elute before/after the main peak (hereafter referred to as *Main*), which elutes at around 31 minutes. In this study, we focused on the physicochemical characterization of six acidic peaks, which, in order of decreasing elution time, are referred to here as *Pre1*, *Pre2*, *Pre3*, *Pre4*, *Pre5*, and *Pre6*, respectively. The *Main* and *Pre* fractions were isolated from the DS by preparative CEX, buffer-exchanged, and concentrated to over 3 mg/mL. These collected fractions were re-injected for analytical CEX to check the purity (Fig. 1B). The isolated *Main* fraction was found to be free of acidic and basic peaks. Each isolated *Pre* fraction still contained a small amount of *Main* peak, but was subjected to subsequent characterization without further purification.

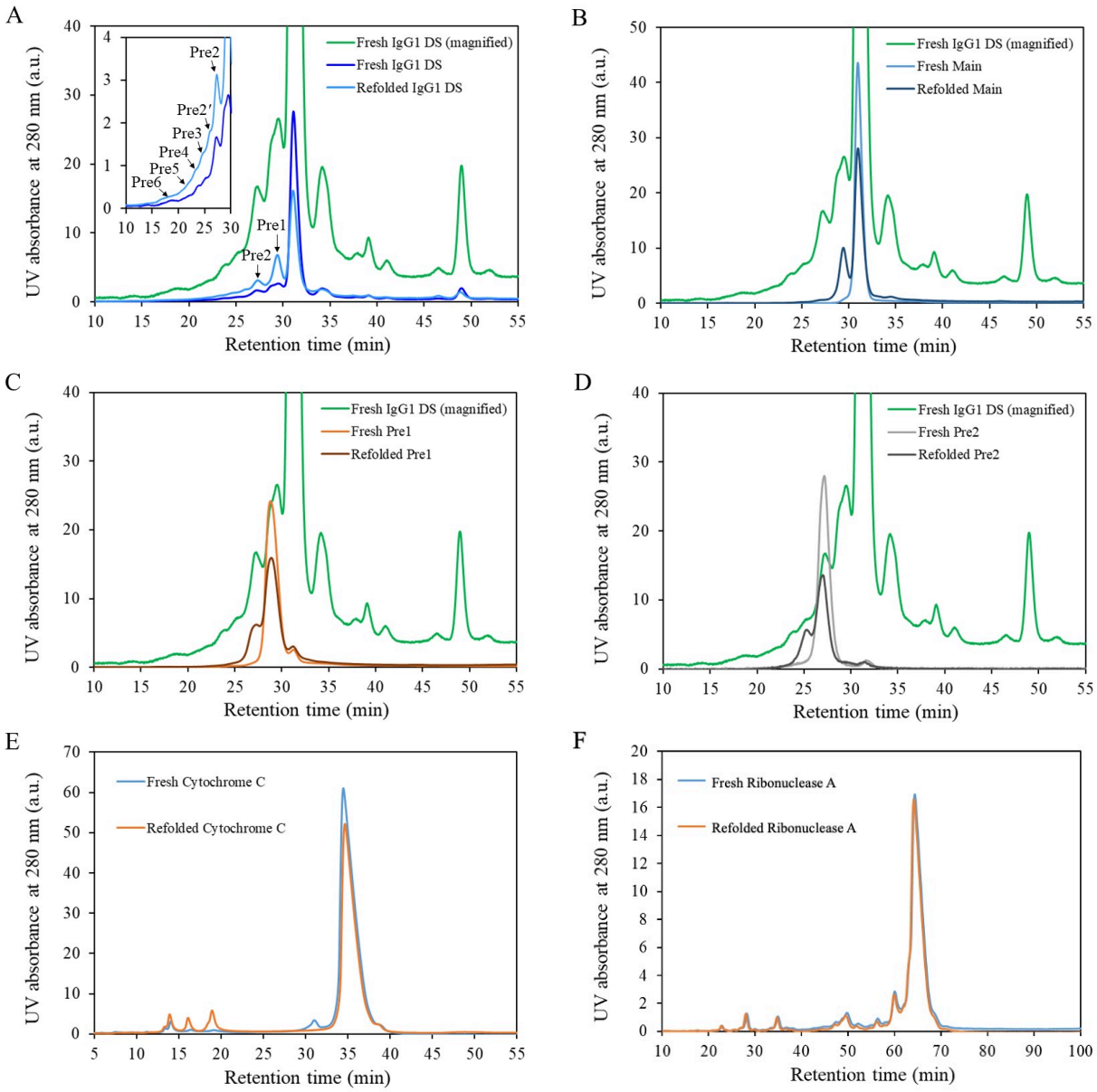

Fig. 3. CEX profiles of fresh (i.e., non-treated) and refolded **(A)** IgG1 drug substance (DS), **(B)** *Main*, **(C)** *Pre1*, **(D)** *Pre2*, **(E)** cytochrome C, and **(F)** ribonuclease A. The magnified CEX profile of the IgG1 DS is shown in **A**, **B**, **C**, and **D** as a reference. Inset in **A** depicts magnified elution profiles from 10 to 30 minutes. The refolding procedure is outlined in Figure 2.

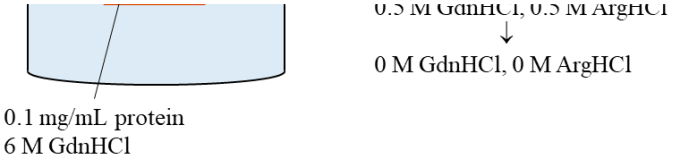

dialysis (GdnHCl: guanidine hydrochloride, ArgHCl: arginine hydrochloride).

To clarify whether the *Pre* peaks corresponded to conformational variants, we performed refolding experiments without a reducing agent. The IgG1 DS and isolated fractions were subjected to denaturation using 6 M guanidine hydrochloride, and were then refolded by stepwise dialysis as outlined in Figure 2. The concentration of guanidine hydrochloride was gradually reduced and 0.5 M arginine hydrochloride was utilized to suppress the formation of aggregates during the refolding process [23, 24]. The protein concentration was set as low as possible (i.e., 0.1 mg/mL) to avoid the formation of aggregates.

CEX profiles of fresh (i.e., non-treated) and refolded IgG1 DS are shown in Figure 3A. Following refolding, the area of the *Main* peak decreased, and that of each *Pre* peak increased. The longer the retention time of *Pre*, the greater the increase. A new peak that was not detected in the fresh IgG1 DS was

generated between the *Pre2* and *Pre3* peaks (depicted as *Pre2'* in Fig. 3A) after refolding. The total peak area of the samples was not changed during the refolding process (the ratio of refolded to fresh is 1.01), suggesting that almost no aggregates were generated under the refolding conditions. The isolated *Main* and *Pre* fractions were also each subjected to the refolding process to examine the changes in CEX profile. The CEX profiles of fresh and refolded *Main* fractions are shown in Figure 3B. The peak area of *Main* decreased, and *Pre1* and a small amount of *Pre2* were generated. *Pre1* generated from the *Main* fraction by the refolding process exhibited a symmetrical peak shape, whereas the *Pre1* peak in the fresh IgG1 DS was asymmetric, suggesting that the *Pre1* fraction contains multiple components with conformational variant being just one of them. Similarly, the isolated *Pre1* and *Pre2* fractions were refolded and analyzed by CEX (Fig. 3C and 3D). *Pre2* and *Pre3* peaks were generated from the *Pre1* and *Pre2* fractions, respectively. A *Main* peak was not generated from the *Pre1* and *Pre2* fractions.

To investigate whether the generation of acidic peaks by refolding is a general phenomenon that could occur in other proteins as well, we subjected cytochrome C and ribonuclease A to the same refolding process and CEX analysis (Fig. 3E and 3F). In cytochrome C, as in the IgG1 DS, the area of the main peak decreased, and the areas of the acidic peaks increased. An acidic peak eluting at around 31 minutes disappeared. In ribonuclease A, the CEX profile was not changed by the refolding process.

These results suggest that the acidic peaks in the IgG1 DS are conformational variants and that such variants could be generated in other proteins. To elucidate the conformational changes occurring in the *Pre* fractions, we characterized them using the following methods.

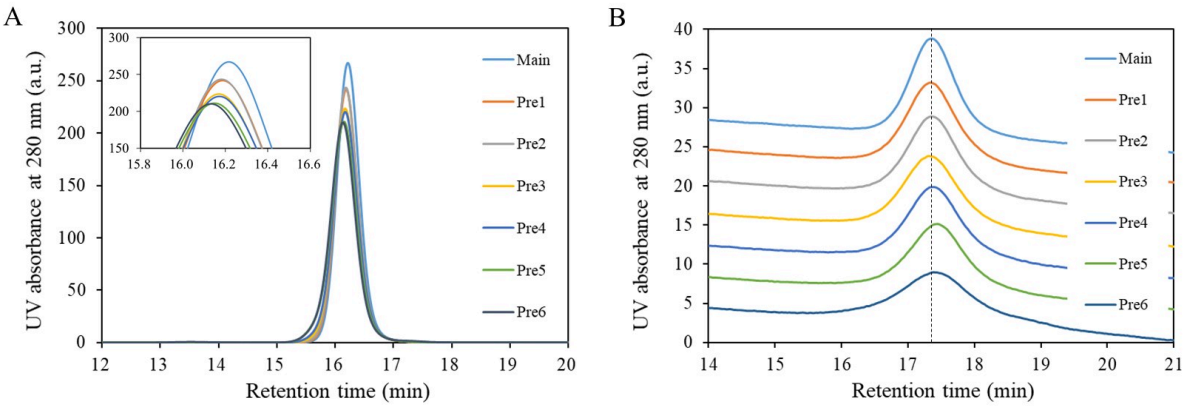

Fig. 4. **(A)** SEC and **(B)** HIC profiles of isolated *Main*, *Pre1*, *Pre2*, *Pre3*, *Pre4*, *Pre5*, and *Pre6* fractions. Inset in **A** depicts magnified elution profiles from 15.8 to 16.6 minutes. Dotted line in **B** shows the retention time of peak of *Main*.

3.3 SEC and HIC analysis

The isolated *Main* and *Pre* fractions were analyzed by SEC. All samples eluted as a single mAb monomer peak and no oligomers or aggregates such as dimers were detected (Fig. 4A). The shorter the elution time of *Pre* in CEX, the broader the monomer peak and the slightly shorter the elution time in SEC, suggesting that the conformational change of *Pre* variants altered their interaction with the SEC column resin or that the conformation of the *Pre* variants was slightly expanded compared to that of the *Main* variant. The isolated *Main* and *Pre* fractions were also analyzed by HIC (Fig. 4B). Similar to the SEC profiles, the shorter the elution time of *Pre* in CEX, the broader the peak in HIC. The retention times of *Pre4*, *Pre5*, and *Pre6* were slightly greater than that of *Main*, indicating that these *Pre* variants were slightly more hydrophobic than the *Main* variant.

Table 1 Hydrodynamic radius [R_h (nm)], radius of gyration [R_g (nm)], maximum dimension [D_{max} (nm)], and χ^2 of fit to the theoretical SAXS profile of isolated *Main*, *Pre1*, *Pre2*, *Pre3*, *Pre4*,

3.4 DLS and SAXS analysis

The R_h values of each fraction were determined by DLS measurements (Table 1). No difference in hydrodynamic properties were detected by DLS, and all samples showed the same R_h values (i.e., 5.3 nm), which is consistent with the R_h values reported for an IgG1 monomer [25]. SAXS profiles and the $p(r)$ functions of each fraction obtained at 20°C are displayed in Figure 5A and Figure 5B, respectively. The

[*a] obtained by DLS measurements at a concentration of 0.5 mg/mL at 25°C. Data represent the mean ± SD of three experiments.

[*b] obtained by SAXS measurements at a concentration of 1 mg/mL at 20°C.

[*c] obtained by fitting to the theoretical scattering profile from the crystal structure of a human IgG1 (pdb code:1hzh.pdb) with the ATSAS program CRYSOL [22].

SAXS profiles and $p(r)$ were typical of monomeric IgG1 [26] and no marked differences were detected between the *Main* and *Pre* fractions. The scattering profiles were compared to the theoretical scattering profile from the crystal structure of a human IgG1 (pdb code:1hzh.pdb) with the ATSAS program CRYSOL. The obtained χ^2 values are listed in Table 1 and range 1.3 to 1.6 suggesting a good agreement between the solution structure and model. The value of R_g and D_{max} were within the error estimates for different fractions (Table 1). These results suggest that the conformational changes occurring in the *Pre* variants are minor.

3.5 DSF analysis

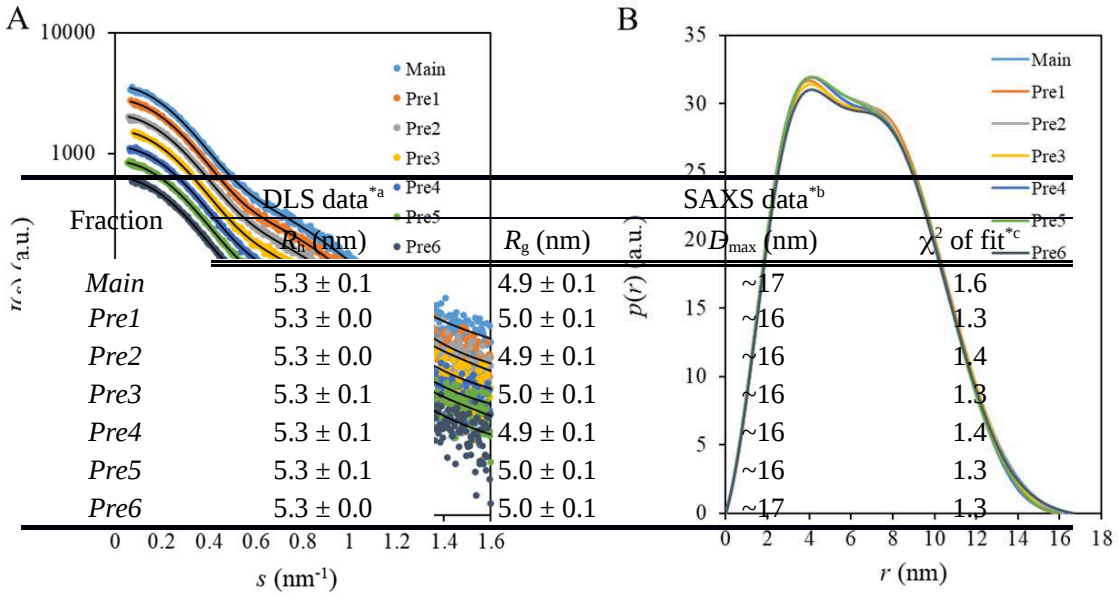

Fraction	DLS data*a R_h (nm)	R_g (nm)	SAXS data*b D_{max} (nm)	χ^2 of fit*c
Main	5.3 ± 0.1	4.9 ± 0.1	~17	1.6
Pre1	5.3 ± 0.0	5.0 ± 0.1	~16	1.3
Pre2	5.3 ± 0.0	4.9 ± 0.1	~16	1.4
Pre3	5.3 ± 0.1	5.0 ± 0.1	~16	1.3
Pre4	5.3 ± 0.1	4.9 ± 0.1	~16	1.4
Pre5	5.3 ± 0.1	5.0 ± 0.1	~16	1.3
Pre6	5.3 ± 0.0	5.0 ± 0.1	~17	1.3

Fig. 5. (A) SAXS profiles of isolated *Main*, *Pre1*, *Pre2*, *Pre3*, *Pre4*, *Pre5*, and *Pre6* fractions (1 mg/mL) at 20°C. The scattering data of *Pre* fractions were shifted downwards in logarithmic scale to avoid overlapping. Solid lines are the result of fitting by indirect Fourier transformation. **(B)** the pair–distance distribution function [$p(r)$].

For the IgG1 used in this study, thermal denaturation of the CH2, CH3, and Fab domains occurs separately in order of increasing temperature [27]. To clarify which domains potentially undergo conformational changes in the *Pre* variants, the T_m of each domain of the *Main* and *Pre* fractions was determined by DSF and compared. DSF thermograms of each fraction at pH 6.1 and pH 4.1 are shown in Figure 6A and Figure 6B, respectively. At pH 6.1, the T_m of the Fab domain exceeded the upper temperature limit of the instrument, and consequently the thermal denaturation of only the two domains of CH2 and CH3 could be detected; however, because the T_m of these domains decreases with the reduction in pH, the thermal denaturation of the three domains of CH2, CH3, and Fab could be detected at pH 4.1. The thermal denaturation curves almost overlapped between the samples, but slight differences between the *Main* and *Pre* fractions were detected in the CH2 and Fab domains. The T_m of the CH2 and CH3 domains at pH 6.1 are shown in Figure 6C and 6D, and the T_m of the CH2, CH3, and Fab domains at pH 4.1 are shown in Figure 6E, 6F, and 6G. The T_m of the CH2 domain of the *Pre* fractions was slightly lower than that of the

Main fraction at both pH values, but no marked difference was detected between the *Main* and *Pre* fractions in the CH3 domain. The T_m of Fab domain tended to be lower in the *Pre* fractions than in the *Main* fraction at pH 4.1, but the difference was extremely small. These results suggest that the conformational changes of the *Pre* variants are minor and occur at multiple sites, at least across the CH2 and Fab domains.

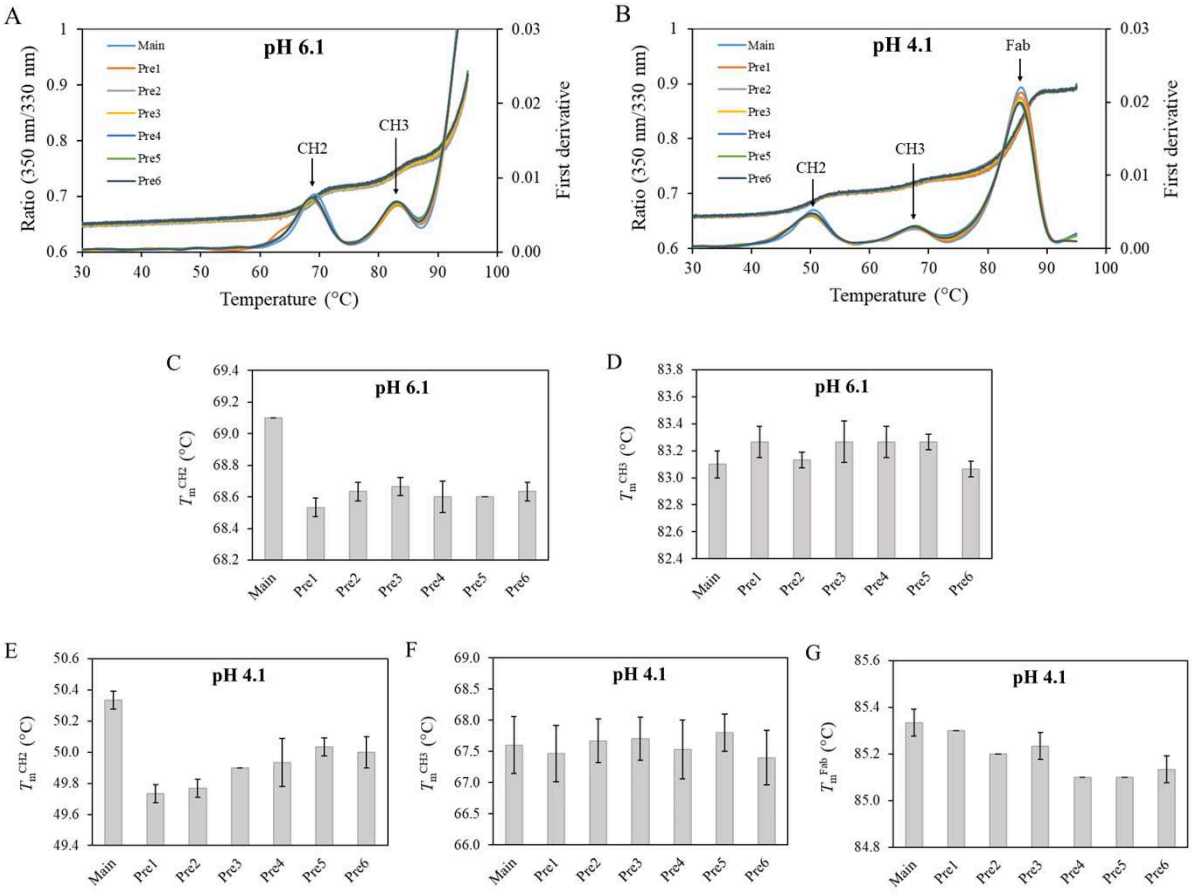

Fig. 6. DSF thermograms of isolated *Main*, *Pre1*, *Pre2*, *Pre3*, *Pre4*, *Pre5*, and *Pre6* fractions (0.5 mg/mL) at **(A)** pH 6.1 and **(B)** pH 4.1. The y-axes represent the ratio of intrinsic fluorescence at emission wavelengths of 330 and 350 nm (350 nm/330 nm) and the first derivative. Each curve represents the mean of three experiments. The peaks of the first derivative correspond to the thermal denaturation of CH2, CH3, and Fab domains in order of increasing temperature. The T_m (°C) of **(C)** CH2 and **(D)** CH3 domains at pH 6.1. The T_m of **(E)** CH2, **(F)** CH3, and **(G)** Fab domains at pH 4.1. Each column represents the mean ± SD of three experiments.

3.6 ANS and intrinsic fluorescence analysis

To further investigate the conformational changes occurring in the *Pre* variants, the hydrophobicity of each fraction was evaluated by ANS, a fluorescent probe that binds to hydrophobic regions. The ANS fluor

Fig. 7. **(A)** ANS fluorescence spectra of isolated *Main*, *Pre1*, *Pre2*, *Pre3*, *Pre4*, *Pre5*, and *Pre6* *Pre* fractions at 25°C. The concentrations of ANS and IgG1 were 200 μM and 2.7 mg/mL, respectively. The excitation wavelength was 385 nm. The fluorescence intensity was normalized to the intensity of the *Main* sample at 494 nm. Each curve represents the mean of three experiments. **(B)** Normalized fluorescence intensity at 494 nm and **(C)** λ_{max} (nm). Each column represents the mean ± SD of three experiments.

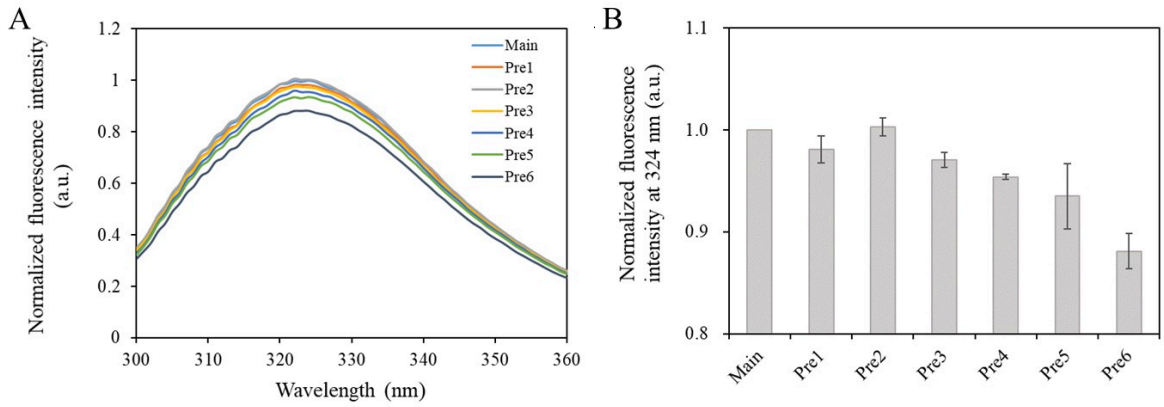

B

fractions at 25°C. The concentration of IgG1 was 3 mg/mL. The excitation wavelength was 285 nm. The fluorescence intensity was normalized by the maximum intensity of the *Main* sample. Each curve represents the mean of three experiments. **(B)** Normalized fluorescence intensity at 324 nm. Each column represents the mean ± SD of three experiments.

emission wavelength (λ_{max}) of ANS in the *Pre* fractions was slightly blue-shifted compared to that of the *Main* fraction. Subsequently, environmental changes around aromatic residues were investigated by intrinsic fluorescence measurements. The intrinsic fluorescence spectra under excitation at 285 nm are shown in Figure 8A. The fluorescence intensity tended to decrease slightly as the *Pre*-fraction number increased (Fig. 8B).

4. Discussion

As previous characterization studies on charge variants of therapeutic mAbs have shown, the full characterization of post-translational modifications in acidic variants of mAbs is challenging and remains an open area of investigation [9, 14–16]. It is usually found that quantitative measurements of identified acidic species leave some gaps, and that the sum of the identified acidic species does not fully account for the total acidic regions in the elution profile. Neill et al. reported that the basic variants of a mAb detected by CEX could be all fully accounted for by identified post-translational modifications, whereas the acidic variants could only be partially explained by deamidation and isomerization [9]. Dada et al. characterized both the acidic and basic regions of imaged capillary isoelectric focusing profile of an IgG1 mAb by using

preparative immobilized pH gradient isoelectric focusing fractionation and reported that unlike the basic variants where the detected modifications are discrete and exclusive, all acidic peaks to a varying degree shared similar modifications [16].

As described in Introduction section, the acidic fractions of the IgG1 mAb used in this study have also been extensively characterized previously by various techniques. However, interestingly, most of them showed no differences from the *Main* fraction (unpublished results). Since few post-translational modifications were detected, we speculated that the main attributes characterizing these unidentified acidic variants would be alterations in their higher order structure. Interestingly, Gervais et al. report that, on the basis of capillary isoelectric focusing, liquid chromatography-mass spectrometry, and liquid chromatography-tandem mass spectrometry data, the acidic variants of L-asparaginase do not include primary sequence modifications (such as deamidation), and they concluded on the basis of SAXS and ion mobility-mass spectrometry data showing slight conformational differences between the acidic and main peaks that the most prevalent acidic peak is a conformational variant [17]. That consideration was further supported by the results of refolding experiments demonstrating that the acidic peak could be converted into the main peak after unfolding using 8M urea and 2.2 M N-ethylurea and refolding by dialysis against water [17]. Even such a small conformational change may alter the overall surface charge distribution, owing to changes in the local distribution of charged residues. With reference to the study by Gervais et al., in this study we investigated whether conformational changes occur in the unidentified acidic variants of IgG1, and we analyzed the conformational changes occurring in the acidic fractions in more detail.

First, we examined whether refolding without a reducing agent could generate the acidic variants of IgG1. By applying stepwise dialysis, the use of arginine hydrochloride during refolding [23, 24], and a low concentration of the IgG1, we found conditions under which the IgG1 could be refolded without aggregation formation and under which the acidic variants could be generated. The results of the refolding studies revealed that the unidentified acidic variants of IgG1 would be conformational variants. Interestingly, *Pre1* was generated from *Main*, *Pre2* was generated from *Pre1*, and *Pre3* was generated from *Pre2* by the refolding process, suggesting that the acidity of the IgG1 molecular surface increased in a stepwise pattern as certain conformational changes accumulated in the *Main* molecule and these variants were eluted as multiple *Pre* peaks depending on the degree of accumulation of the conformational changes. The fact that only a small amount of *Pre2* and no *Pre3* were generated from *Main* is likely due to the low

probability of multiple conformational changes occurring simultaneously within a single molecule. With L-asparaginase, the refolding process generated the main peak from the acidic peak [17], but this was not the case for the IgG1 used in this study, presumably because the activation energy barrier for changing from *Pre* variants to the *Main* variant is very high in IgG1. The *Pre1* peak generated from *Main* by refolding process was symmetric. On the other hand, the *Pre1* peak originally contained in the IgG1 DS was asymmetric, which is likely due to the presence of sialylated IgG1 as described in Introduction section in addition to the conformational variant.

SAXS experiments were performed to investigate the conformational changes occurring in the *Pre* variants, but no marked differences in SAXS profiles were detected between the *Main* and *Pre* fractions, unlike in the case of L-asparaginase [17]. As well, no difference was detected between the *Main* and *Pre* fraction's R_h measured by DLS. These results indicate that the conformational changes occurring in the *Pre* variants are likely localized/minor and do not greatly affect the overall global disposition of the IgG1 in solution. Since IgG1 is a multi-domain/modular protein that is present in solution as a population-state ensemble, the minor conformational changes occurring in the *Pre* variants may be difficult to detect by SAXS due to the net averaging of conformational fluctuations. By isolating the Fc and Fab domains after fragmentation by enzyme treatment (such as papain digestion) and comparing the SAXS data between the *Main* and *Pre* fractions, it may be possible to identify those domains in which the conformational changes occur. However, isolating the Fc and Fab domains of the *Pre* fractions for SAXS experiments is time-consuming and labor-intensive; therefore, in this study, the SAXS experiments were limited to the measurement of the whole IgG1. Online CEX–SAXS, which can obtain SAXS data while isolating and purifying each domain using enzyme-treated IgG1, may be a suitable tool for detecting conformational changes occurring in the *Pre* variants [28–30]. Further studies will be required in order to detect the conformational changes in the *Pre* variants using SAXS.

In the SEC, HIC, DSF, and fluorescence analyses, slight differences were observed between the *Main* fraction and the *Pre* fractions, however, the differences detected were extremely small. The results of HIC and ANS fluorescence showed that the *Pre* variants were slightly more hydrophobic than the *Main* variant. In DSF, the T_m of the CH2 and Fab domains were slightly decreased in the *Pre* fractions, suggesting that the conformational changes in the *Pre* variants occur at multiple sites, at least across these two domains. The intrinsic fluorescence intensity of the *Pre* fractions decreased in a CEX retention time–dependent manner,

suggesting that the minor conformational changes of the *Pre* variants occur around aromatic residue regions. Wen et al. reported that microconformational changes within aromatic hydrophobic regions of several representative proteins could be induced by incubation with amine or guanidine additives [31]. Taking into account the results of that study, it could be assumed that, in the *Pre* variants, the side chains of aromatic residues are exposed to water due to local denaturation around the aromatic side chains, resulting in a decrease in the intrinsic fluorescence intensity and an increase in the hydrophobicity of the molecular surface. In SEC, the elution time of the monomer peak was slightly shorter for the *Pre* fractions; considering the results of HIC, fluorometry, and DSF, this was presumably due to the slightly expanded conformation of the *Pre* variants compared to that of the *Main* variant due to local denaturation. This hypothesis is consistent with the results of a previous study, in which SAXS measurements detected a slightly expanded state in the acidic peak of L-asparaginase [17].

For cytochrome C, acidic peaks were also generated by the refolding process. It is interesting to note that conformational variants resulting from the refolding process were detected as acidic peaks rather than basic peaks both in IgG1 and in cytochrome C. One possible explanation is that the exposure of aromatic amino acid side chains to water is induced by local denaturation, resulting in altered interactions with the column resin and the subsequent detection as acidic peaks. However, further studies are needed to clarify the mechanism of this phenomenon. On the other hand, refolding of ribonuclease A did not change the CEX profile, and no acidic peaks were generated. The stability of ribonuclease A is well known. The classical method for purification of ribonuclease A from bovine pancreas relies on its high stability that can maintain its integrity and solubility under severe conditions [32]. Conformational changes such as those seen in this study may be less likely to occur for highly stable proteins such as ribonuclease A.

5. Conclusion

Charge variation is one of the most common forms of heterogeneity in therapeutic mAbs, and thorough characterization of charge variants is important to identify critical quality attributes. However, it is not unusual that the sum of the quantitative values of the identified acidic species does not fully account for the total acidic regions in the elution profile. In this study, acidic variants of IgG1, which had been rarely identified in previous characterizations, were found to be generated by the process of refolding without a

reducing agent, indicating that these acidic variants are conformational variants. On the other hand, no conformational changes were detected by SAXS experiments for the intact IgG1, indicating that the conformational changes are minor. The results of HIC and ANS fluorescence showed that the *Pre* variants were slightly more hydrophobic than the *Main* variant. In DSF, the T_m of the CH2 and Fab domains were slightly decreased in the *Pre* fractions, suggesting that the minor conformational changes in the *Pre* variants occur at multiple sites, at least across these two domains. The intrinsic fluorescence intensity of the *Pre* fractions decreased in a CEX retention time–dependent manner, suggesting that the minor conformational changes of the *Pre* variants occur around aromatic residue regions. Taken together, these results suggest that, in the *Pre* variants, the side chains of aromatic residues are exposed to water due to local denaturation around the aromatic side chains, resulting in a decrease in the intrinsic fluorescence intensity and an increase in the hydrophobicity of the molecular surface. For cytochrome C, acidic peaks were also generated by the refolding process. One possible explanation is that the exposure of aromatic amino acid side chains to water is induced by local denaturation, resulting in altered interactions with the column resin and the subsequent detection as acidic peaks. Further studies are needed to elucidate in more detail the conformational changes, their formation mechanisms, and the mechanisms by which they are detected as acidic variants. This study provides new insights into the characterization of acidic variants of therapeutic mAbs that are not currently fully understood.

Acknowledgements

The authors thank Dr. Kohei Tsumoto (Medical Proteomics Laboratory, Institute of Medical Science, The University of Tokyo) for thoughtful discussions. The authors also thank Atsushi Watanabe, Yuka Funakoshi, So Yamaguchi, Akira Hayasaka, Chifumi Teramoto, and Kinue Shimizu for their support with experiments.

References

[1] H. Liu, G. Gaza-Bulseco, D. Faldu, C. Chumsae, J. Sun, Heterogeneity of monoclonal antibodies, J. Pharm. Sci. 97 (2008) 2426–2447.

[2] C.A. Boswell, D.B. Tesar, K. Mukhyala, F.P. Theil, P.J. Fielder, L.A. Khawli, Effects of charge on antibody tissue distribution and pharmacokinetics, Bioconjug. Chem. 21 (2010) 2153–2163.

[3] K.G. Moorhouse, W. Nashabeh, J. Deveney, N.S. Bjork, M.G. Mulkerrin, T. Ryskamp, Validation of an HPLC method for the analysis of the charge heterogeneity of the recombinant monoclonal antibody IDEC-C2B8 after papain digestion, J. Pharm. Biomed. Anal.

[4] M. Perkins, R. Theiler, S. Lunte, M. Jeschke, Determination of the origin of charge heterogeneity in a murine monoclonal antibody, Pharm. Res. 17 (2000) 1110–1117.

[5] R.J. Harris, B. Kabakoff, F.D. Macchi, F.J. Shen, M. Kwong, J.D. Andya, S.J. Shire, N. Bjork, K. Totpal, A.B. Chen, Identification of multiple sources of charge heterogeneity in a recombinant antibody, J. Chromatogr. B Biomed. Sci. Appl. 752 (2001) 233–245.

[6] S. Chung, J. Tian, Z. Tan, J. Chen, J. Lee, M. Borys, Z.J. Li, Industrial bioprocessing perspectives on managing therapeutic protein charge variant profiles, Biotechnol. Bioeng. 115 (2018) 1646–1665.

[7] J. Vlasak, R. Ionescu, Heterogeneity of monoclonal antibodies revealed by charge-sensitive methods, Curr. Pharm. Biotechnol. 9 (2008) 468–481.

[8] L.A. Khawli, S. Goswami, R. Hutchinson, Z.W. Kwong, J. Yang, X. Wang, Z. Yao, A. Sreedhara, T. Cano, D. Tesar, I. Nijem, D.E. Allison, P.Y. Wong, Y.H. Kao, C. Quan, A. Joshi, R.J. Harris, P. Motchnik, Charge variants in IgG1: Isolation, characterization, in vitro binding properties and pharmacokinetics in rats, MAbs. 2 (2010) 613–624.

[9] A. Neill, C. Nowak, R. Patel, G. Ponniah, N. Gonzalez, D. Miano, H. Liu, Characterization of recombinant monoclonal antibody charge variants using OFFGEL fractionation, weak anion exchange chromatography, and mass spectrometry, Anal. Chem. 87 (2015) 6204–6211.

[10] G. Ponniah, C. Nowak, A. Neill, H. Liu, Characterization of charge variants of a monoclonal antibody using weak anion exchange chromatography at subunit levels, Anal. Biochem. 520 (2017) 49–57.

[11] B. Yan, S. Steen, D. Hambly, J. Valliere-Douglass, T. Vanden Bos, S. Smallwood, Z. Yates, T. Arroll, Y. Han, H. Gadgil, R.F. Latypov, A. Wallace, A. Lim, G.R. Kleemann, W. Wang, A. Balland, Succinimide formation at Asn 55 in the complementarity determining region of a recombinant monoclonal antibody IgG1 heavy chain, J. Pharm. Sci. 98 (2009) 3509–3521.

[12] G.C. Chu, D. Chelius, G. Xiao, H.K. Khor, S. Coulibaly, P.V. Bondarenko, Accumulation of succinimide in a recombinant monoclonal antibody in mildly acidic buffers under elevated temperatures, Pharm. Res. 24 (2007) 1145–1156.

[13] X.C. Yu, K. Joe, Y. Zhang, A. Adriano, Y. Wang, H. Gazzano-Santoro, R.G. Keck, G. Deperalta, V. Ling, Accurate determination of succinimide degradation products using high fidelity trypsin digestion peptide map analysis, Anal. Chem. 83 (2011) 5912–5919.

[14] G. Ponniah, A. Kita, C. Nowak, A. Neill, Y. Kori, S. Rajendran, H. Liu, Characterization of the acidic species of a monoclonal antibody using weak cation exchange chromatography and LC-MS, Anal. Chem. 87 (2015) 9084–9092.

[15] Y.D. Liu, L. Cadang, K. Bol, X. Pan, K. Tschudi, M. Jazayri, J. Camperi, D. Michels, J. Stults, R.J. Harris, F. Yang, Challenges and strategies for a thorough characterization of antibody acidic charge variants, Bioengineering (Basel). 9 (2022) 641.

[16] O.O. Dada, N. Jaya, J. Valliere-Douglass, O. Salas-Solano, Characterization of acidic and basic variants of IgG1 therapeutic monoclonal antibodies based on non-denaturing IEF fractionation, Electrophoresis. 36 (2015) 2695–2702.

[17] D. Gervais, D. King, P. Kanda, N. Foote, L. Elliott, P. Brown, N.O. Lee, K. Thalassinos, C. Pizzey, R. Rambo, T.C. Minshull, M.J. Dickman, S. Smith, Structural characterisation of non-deamidated acidic variants of *Erwinia chrysanthemi* L-asparaginase using small-angle X-ray scattering and ion-mobility mass spectrometry, Pharm. Res. 32 (2015) 3636–3648.

[18] C.E. Blanchet, A. Spilotros, F. Schwemmer, M.A. Graewert, A. Kikhney, C.M. Jeffries, D. Franke, D. Mark, R. Zengerle, F. Cipriani, S. Fiedler, M. Roessle, D.I. Svergun, Versatile sample environments and automation for biological solution X-ray scattering experiments at the P12 beamline (PETRA III, DESY). J. Appl. Crystallogr. 48 (2015) 431–443.

[19] A. Round, F. Felisaz, L. Fodinger, A. Gobbo, J. Huet, C. Villard, C.E. Blanchet, P. Pernot, S. McSweeney, M. Roessle, D.I. Svergun, F. Cipriani, BioSAXS Sample Changer: a robotic sample changer for rapid and reliable high-throughput X-ray solution scattering experiments. Acta. Crystallogr. D Biol. Crystallogr. 71 (2015) 67–75.

[20] D. Franke, A.G. Kikhney, D.I. Svergun, Automated acquisition and analysis of small angle X-ray scattering data. Nucl. Inst. Meth. A. 689 (2012) 52–59.

[21] D.I. Svergun, Determination of the regularization parameter in indirect-transform methods using perceptual criteria. J. Appl. Crystallogr. 25 (1992) 495–503.

[22] D. Svergun, C. Barberato, M.H.J. Koch, CRYSOL–a program to evaluate X-ray solution scattering of biological macromolecules from atomic coordinates. J. Appl. Crystallogr. 28 (1995) 768–773.

[23] K. Tsumoto, K. Shinoki, H. Kondo, M. Uchikawa, T. Juji, I. Kumagai, Highly efficient recovery of functional single-chain Fv fragments from inclusion bodies overexpressed in *Escherichia coli* by controlled introduction of oxidizing reagent--application to a human single-chain Fv fragment. J. Immunol. Methods. 219 (1998) 119–129.

[24] M. Umetsu, K. Tsumoto, M. Hara, K. Ashish, S. Goda, T. Adschiri, I. Kumagai, How additives influence the refolding of immunoglobulin-folded proteins in a stepwise dialysis system. Spectroscopic evidence for highly efficient refolding of a single-chain Fv fragment. J. Biol. Chem. 278 (2003) 8979–8987.

[25] R. Bauer, A. Müller, M. Richter, K. Schneider, J. Frey, W. Engelhardt, Influence of heavy metal ions on antibodies and immune complexes investigated by dynamic light scattering and enzyme-linked immunosorbent assay. Biochim. Biophys. Acta. 1334 (1997) 98–108.

[26] W.G. Lilyestrom, S.J. Shire, T.M. Scherer, Influence of the cosolute environment on IgG solution structure analyzed by small-angle X-ray scattering. J. Phys. Chem. B. 116 (2012) 9611–9618.

[27] D. Kameoka, E. Masuzaki, T. Ueda, T. Imoto, Effect of buffer species on the unfolding and the aggregation of humanized IgG. J. Biochem. 142 (2007) 383–391.

[28] S. Hutin, M. Brennich, B. Maillot, A. Round, Online ion-exchange chromatography for small-angle X-ray scattering. Acta. Crystallogr. D Struct. Biol. 72 (2016) 1090–1099.

[29] M.E. Brennich, A.R. Round, S. Hutin, Online size-exclusion and ion-exchange chromatography on a SAXS beamline. J. Vis. Exp. 119 (2017) 54861.

[30] P.V. Konarev, M.A. Graewert, C.M. Jeffries, M. Fukuda, T.A. Cheremnykh, V.V. Volkov, D.I. Svergun, EFAMIX, a tool to decompose inline chromatography SAXS data from partially overlapping components. Protein Sci. 31 (2022) 269–282.

[31] L. Wen, M. Lyu, H. Xiao, H. Lan, Z. Zuo, Z. Yin, Protein aggregation and performance optimization based on microconformational changes of aromatic hydrophobic regions. Mol. Pharm. 15 (2018) 2257–2267.

[32] R.T. Raines, Ribonuclease A. Chem. Rev. 98 (1998) 1045–1066.

Author contributions

Masakazu Fukuda: Conceptualization, Data curation, Formal analysis, Investigation, Methodology, Writing – original draft. **Melissa A. Graewert:** Data curation, Formal analysis, Investigation, Methodology, Writing – review and editing. **Cy M. Jeffries:** Formal analysis, Investigation, Methodology, Writing – review and editing. **Dmitri I. Svergun:** Project administration, Resources, Writing – review and editing. **Tadao Yamazaki:** Resources, Writing – review and editing. **Akiko Koga:** Conceptualization, Supervision, Writing – review and editing. **Yuji Yamanaka:** Project administration, Writing – review and editing.

Subject Category: Protein structure and analysis

Small conformational changes in IgG1 detected as acidic charge variants by cation exchange chromatography

Masakazu Fukuda[a,b,*] · Melissa A. Graewert[c] · Cy M. Jeffries[c] · Dmitri I. Svergun[c] · Tadao Yamazaki[a] · Akiko Koga[a] · Yuji Yamanaka[a]

[a] *Production Engineering Department, Chugai Pharmaceutical Co., Ltd.,*
5-5-1 Ukima, Kita-ku, Tokyo 115-8543, Japan

[b] *Laboratory of Functional Molecular Chemistry, Kobe Pharmaceutical University,*
4-19-1, Motoyamakita-machi, Higashinada-ku, Kobe 658-8558, Japan

[c] *European Molecular Biology Laboratory (EMBL) Hamburg Unit, c/o Deutsches Elektronen Synchrotron (DESY), 22607 Hamburg, Germany*

[*] Corresponding author.
E-mail address: fukudamk@kobepharma-u.ac.jp (M. Fukuda).

ABSTRACT

Fully characterizing the post-translational modifications present in charge variants of therapeutic monoclonal antibodies (mAbs), particularly acidic variants, is challenging and remains an open area of investigation. In this study, to test the possibility that chromatographically separated acidic fractions of therapeutic mAbs contain conformational variants, we undertook a mAb refolding approach using as a case study an IgG1 that contains many unidentified acidic peaks with few post-translational modifications, and examined whether different acidic peak fractions could be generated corresponding to these variants. The IgG1 drug substance was denatured by guanidine hydrochloride, without a reducing agent present, and gradually refolded by stepwise dialysis against arginine hydrochloride used as an aggregation suppressor. Each acidic chromatographic peak originally contained in the IgG1 drug substance was markedly increased by this stepwise refolding process, indicating that these acidic variants are conformational variants. However, no conformational changes were detected by small-angle X-ray scattering experiments for the whole IgG1, indicating that the conformational changes are minor. Chromatographic, thermal and fluorescence analyses suggested that the conformational changes are a localized denaturation effect centred around the aromatic amino acid regions. This study provides new insights into the characterization of acidic variants that are currently not fully understood.

Keywords:

Acidic variant

Cation-exchange chromatography

Conformational change

Monoclonal antibody

Refolding

Abbreviations

ANS	1-Anilino-8-naphthalene sulfonate
CEX	Cation-exchange chromatography
DSF	Differential scanning fluorimetry
DS	Drug substance
DLS	Dynamic light scattering
R_h	Hydrodynamic radius
HIC	Hydrophobic interaction chromatography
D_{max}	Maximum dimension
λ_{max}	Maximum emission wavelength
$p(r)$	Pair–distance distribution function
R_g	Radius of gyration
SEC	Size-exclusion chromatography
SAXS	Small-angle X-ray scattering
T_m	Thermal denaturation temperature

1. Introduction

Therapeutic monoclonal antibodies (mAbs), like other proteins, are susceptible to chemical and enzymatic post-translational modifications during their manufacture, resulting in a heterogeneous mix of variants containing various post-translational modifications [1]. One of the most common forms of heterogeneity is charge variation, and thorough characterization of charge variants is important in order to identify critical quality attributes. Ion-exchange chromatography is the gold standard method for charge variant analysis. Cation-exchange chromatography (CEX) is the default method because many therapeutic mAbs have basic isoelectric points [2]. Isoelectric focusing is also employed, where the separation is based on the net charge of the protein. However, isoelectric focusing is less sensitive to the localized charge distribution on the protein surface. Charge variants with the same isoelectric point by isoelectric focusing have been reported to show multiple peaks when analyzed by chromatographic techniques [3–5], suggesting that net charge is not the only factor affecting the chromatographic behavior, and that localized charge distribution and stereochemistry may alter the chromatographic elution profiles in subtle ways [6].

Charge variants are classified as either acidic or basic relative to the main variant. Acidic variants exhibit an isoelectric point lower than that of the main variant and elute earlier than the main peak when analyzed by CEX, whereas basic variants exhibit a higher isoelectric point and elute later. Various post-translational modifications have been reported to contribute to the formation of acidic and basic variants [6–9]. Post-translational modifications that can lead to the formation of acidic variants include sialylation, asparagine deamidation, glycation, and C-terminal lysine cleavage. Factors that can lead to the formation of basic variants include the presence of C-terminal lysine, N-terminal glutamine, C-terminal amidation, isomerization, and succinimide formation. Some post-translational modifications directly alter the net charge of the proteins while others induce conformational changes that affect the local charge distribution. Interestingly, Ponniah et al. reported succinimide species eluting as acidic variants in anion-exchange chromatography [10], contrary to previous reports of succinimide species being classified as basic variants [11–13]. A difference in net charge cannot explain the elution of succinimide species as acidic variants, and the authors of that report suggested that succinimide formation causes a conformational change, which leads to differences in surface charge distribution.

Although several types of post-translational modification have already been identified in various mAbs, the full characterization of post-translational modifications in charge variants of mAbs, particularly acidic variants, is challenging and remains an open area of investigation [9, 14–16]. It is usually found that the sum of the quantitative values of the identified acidic species does not fully account for the total acidic regions in the elution profile. We previously characterized acidic variants of an IgG1 mAb internally by using standard techniques, but we could hardly detect differences between the main peak fraction and the acidic peak fractions (unpublished results). Briefly, sialidase digestion partially decreased the area of the most prevalent acidic peak and increased the area of the main peak, indicating that the acidic peak is only partially composed of IgG1 containing terminal sialic acid on the Fc N-glycans. Glycation was not identified as a main attribute because the decrease in the peak areas of the acidic fractions by enzymatic deglycosylation with PNGase F was limited to the effect of sialylation. The deglycosylated main and acidic fractions were reduced and carboxymethylated, and then the molecular weights of their heavy and light chains were determined by liquid chromatography-mass spectrometry. As a result, the two molecular weights were found to be completely identical between the main and acidic fractions. Furthermore, trypsin peptide mapping of the deglycosylated main and acidic fractions revealed that the acidic variants do not include primary sequence modifications (such as deamidation). The most probable cause of this gap may be slight conformational differences that are difficult to detect. Interestingly, Gervais et al. report that, based on results of extended characterization and refolding studies, the most prevalent acidic peak of *Erwinia chrysanthemi* L-asparaginase (a 140-kDa homotetramer in its active form) is a conformational variant with no primary sequence modifications [17].

In this study, to test the possibility that the acidic fractions of therapeutic mAbs contain conformational variants, we examined whether additional acidic peaks could be generated by a refolding process without a reducing agent, using as an example the aforementioned IgG1 mAb that contains many unidentified acidic peaks with few post-translational modifications. Since acidic peaks were generated by the refolding process, we considered these acidic peaks as conformational variants and examined the conformational changes that occur in the acidic fraction using various analytical methods.

2. Materials and methods

2.1 Materials

The drug substance (DS) used in this study was a humanized IgG1 mAb to human interleukin-6 receptor, manufactured by Chugai Pharmaceutical (Tokyo, Japan). The theoretical isoelectric point of the IgG1 was 9.3. Cytochrome C from equine heart and ribonuclease A from bovine pancreas were purchased from Merck (Darmstadt, Germany). 2-Morpholinoethanesulfonic acid monohydrate (MES) was purchased from Dojindo Laboratories (Kumamoto, Japan). 1-Anilino-8-naphthalene sulfonate (ANS) was purchased from Cayman Chemical (Ann Arbor, MI, USA). All other chemicals were purchased from Fujifilm Wako Pure Chemical Corporation (Osaka, Japan). The protein samples were formulated in a buffer of 25 mM MES/NaOH, 150 mM NaCl, pH 6.1, unless otherwise noted. The protein concentration was determined using UV absorbance at 280 nm.

2.2 Protein refolding by stepwise dialysis

The IgG1 DS, cytochrome C and ribonuclease A, as well as the main and acidic peak fractions isolated from the IgG1 DS by preparative CEX described below were used in refolding studies without a reducing agent, where all unfolding/refolding steps were maintained at pH 6.1 and performed at room temperature (nominally 23°C). The protein samples were unfolded in the MES formulation buffer in the presence of 6 M guanidine hydrochloride at a protein concentration of 0.1 mg/mL for 1 hour. The guanidine hydrochloride was gradually removed to refold the protein by stepwise dialysis using a Slide-A-Lyzer dialysis cassette (20,000 MWCO for IgG1 samples; 3,500 MWCO for cytochrome C and ribonuclease A samples; Thermo Fisher Scientific, Waltham, MA, USA) against 100-fold volume excess of MES formulation buffer with 0.5 M arginine hydrochloride in combination with systematically decreasing concentrations of guanidine hydrochloride (i.e., 3 M, 2 M, 1 M, and 0.5 M) for more than 6 hours each, followed by a final dialysis step against the MES formulation buffer without arginine hydrochloride or guanidine hydrochloride for more than 18 hours.

2.3 Cation-exchange chromatography (CEX)

The main and acidic mAb peak fractions were isolated from the IgG1 DS by preparative CEX, using a Dionex UltiMate 3000 HPLC system (Thermo Fisher Scientific) equipped with a semi-preparative column,

Propac WCX-10 (9.0×250 mm, 10 μm, Thermo Fisher Scientific). Mobile phase A consisted of 25 mM MES/NaOH, pH 6.1 while mobile phase B was 25 mM MES/NaOH, 250 mM NaCl, pH 6.1. The IgG1 DS was diluted with mobile phase A and injected onto the column at a concentration of 22.5 mg/mL. The injection volume was 160 μL, where the column flow-rate was maintained at 1 mL/min throughout the ion exchange, and performed at 40°C. After sample injection, the column was run for 5 minutes using a mobile phase ratio of 63% v/v A and 37% v/v B followed by a linear elution gradient of 0.4% v/v mobile phase B per minute, ending at 50 minutes. The column was then washed for 10 minutes with 100% B. The protein elution was monitored by UV absorbance at 280 nm. Each collected sample was buffer-exchanged into the standard formulation buffer of 25 mM MES/NaOH, 150 mM NaCl, pH 6.1 and concentrated to over 3 mg/mL using Amicon Ultra filters (50,000 MWCO; Merck).

The elution profiles of IgG1, cytochrome C, and ribonuclease A samples were analyzed by analytical CEX, using an Agilent 1290 Infinity HPLC system (Santa Clara, CA, USA) equipped with an analytical weak cation exchange column, ProPac WCX-10 (4.0×250 mm, 10 μm, Thermo Fisher Scientific). Except as described below, the methods were the same as those for preparative CEX. Before chromatographic analysis, the protein samples were buffer-exchanged into mobile phase A and concentrated as needed by centrifugation using Amicon Ultra filters (50,000 MWCO for IgG1 samples, 3000 MWCO for cytochrome C and ribonuclease A samples; Merck). The protein samples were injected at a concentration of 0.5 mg/mL. The injection volumes were 30 μL for the IgG1 samples and 100 μL for cytochrome C and ribonuclease A, maintaining a flow rate of 0.5 mL/min at room temperature. For the IgG1 samples, after running the column for 5 minutes with 63% v/v A and 37% v/v B, a linear elution gradient of 0.4% v/v mobile phase B per minute was applied out to 80 minutes. For cytochrome C, a linear elution gradient of 0.4% v/v B per minute was applied after running the column at 46% v/v A and 54% v/v B for 5 minutes, ending at 55 minutes. For ribonuclease A, a linear elution gradient of 0.2% v/v B per minute was used after running the column at 67% v/v A and 33% v/v B for 5 minutes, for a total of 100 minutes (in this case, mobile phase B consisted of 25 mM MES/NaOH, 500 mM NaCl, pH 6.1). In all instances, and at the completion of the CEX gradient, the column was washed for 5 minutes with 100% v/v of the respective mobile phase B.

2.4 Size-exclusion chromatography (SEC)

The elution profiles of IgG1 samples were analyzed by SEC at room temperature, using an Agilent 1290 Infinity HPLC system equipped with a size exclusion column, TSK-gel G3000SW$_{XL}$ (7.8×300 mm, 5 μm, Tosoh, Tokyo, Japan). The IgG1 samples were injected at a concentration of 1 mg/mL, with an injection volume of 40 μL. A running buffer of 50 mM sodium phosphate, 300 mM NaCl, pH 7.0 was used at a flow rate of 0.5 mL/min. The protein elution was monitored by UV absorbance at 280 nm.

2.5 Hydrophobic interaction chromatography (HIC)

The elution profiles of the IgG1 samples were analyzed by HIC using an Agilent 1290 Infinity HPLC system equipped with a hydrophobic interaction column, ProPac HIC-10 (4.6×100 mm, 5 μm, Thermo Fisher Scientific). Before chromatographic analysis, the IgG1 samples were buffer-exchanged into a buffer of 25 mM MES/NaOH, pH 6.1 and concentrated as needed by centrifugation using Amicon Ultra filters (50,000 MWCO; Merck). The protein samples were injected at a concentration of 0.4 mg/mL. The injection volume was 10 μL. Mobile phase A was 100 mM sodium phosphate, pH 6.1. Mobile phase B was 100 mM sodium phosphate, 2 M $(NH_4)_2SO_4$, pH 6.1. The flow rate was set to 0.5 mL/min and the analysis was performed at room temperature. A linear elution gradient of 2% mobile phase A per minute was applied after running the column at 50% v/v A and 50% v/v B for 5 minutes, and ended at 20 minutes. The column was then washed for 10 minutes with 100% v/v A. The protein elution was monitored by UV absorbance at 280 nm.

2.6 Dynamic light scattering (DLS)

DLS measurements were performed using a DynaPro Plate Reader II (Wyatt Technology Corporation, Santa Barbara, CA, USA) to obtain the average hydrodynamic radius [R_h (nm)] at 25°C. The IgG1 samples were dispensed into a 384-well plate at a concentration of 0.5 mg/mL. The sample volume was 25 μL.

2.7 Small-angle X-ray scattering (SAXS)

SAXS experiments were performed at the EMBL P12 beam line (PETRA III, DESY synchrotron, Hamburg, Germany) [18]. An automated robotic sample changer (BioSAXS; Arinax, Grenoble, France) was employed to deliver the IgG1 samples (1 mg/mL) and corresponding matched buffers at 20°C under continuous flow to the beam line through a 1 mm capillary of the sample exposure unit [19]. Two-

dimensional SAXS patterns were collected using a PILATUS 6M pixel detector, a sample-detector distance of 3.0 m and a wavelength (λ) of 0.124 nm. A momentum transfer range of $0.026 < s < 7.288$ nm^{-1} (where $s = 4\pi\sin\theta/\lambda$, 2θ is the scattering angle) was covered. Data reduction were performed by the automated data pipeline SASFLOW [20]. Briefly, the isotropic two-dimensional scattering intensities were normalized to the intensity of the transmitted beam and azimuthally averaged to generate one-dimensional scattering profiles [$I(s)$ vs s]. Data collection was divided into 20 separate frames of 50 msec each. To exclude data from samples potentially affected by radiation damage, automated pairwise 1D data frame comparisons and subsequent data-frame rejection were employed, followed by undamaged sample frame averaging and buffer scattering subtraction. The radius of gyration (R_g) and extrapolated scattering to zero angle [$I(0)$] was obtained by employing the Guinier approximation [$\ln I(s)$ vs s for $sR_g < 1.3$] as well as the calculation of the scattering pair–distance distribution function [$p(r)$] from which the maximum dimension (D_{max}) was also estimated [21]. The fits to the theoretical scattering profile from the high-resolution crystal structure of a human IgG1 (pdb code:1hzh.pdb) were computed with CRYSOL [22].

2.8 Differential scanning fluorimetry (DSF)

DSF measurements were performed using a Prometheus NT.48 (NanoTemper Technologies, Munich, Germany) with UV transparent capillaries. In the DSF experiments, a buffer condition of 25 mM citrate/NaOH, 150 mM NaCl, pH 4.1 was used in addition to the standard formulation MES buffer at pH 6.1 because the thermal denaturation temperature (T_m) of the Fab domain at pH 6.1 exceeded this instrument's upper measurement temperature (i.e., 95°C). The IgG1 samples were buffer-exchanged into the buffer at pH 4.1 via centrifugation using Amicon Ultra filters (50,000 MWCO; Merck). The IgG1 samples were loaded into the capillaries at a concentration of 0.5 mg/mL. The loading volume was 11 μL. DSF scans were performed at a rate of 1°C/min from 15°C to 95°C. Thermal denaturation was measured by detecting the temperature-dependent changes in the ratio of intrinsic fluorescence at emission wavelengths of 330 and 350 nm (350 nm/330 nm). The T_m was determined from the peaks of the first derivative of the fluorescence ratio. Data were analyzed with ThermControl software (NanoTemper Technologies).

2.9 Fluorescence measurements

Fluorescence measurements were performed with a microplate spectrofluorometer Infinite M1000 (Tecan, Mannedorf, Switzerland). For the ANS fluorescence measurements, a concentrated stock solution of ANS (2 mM ANS in the standard formulation MES buffer) was added to each IgG1 sample (3 mg/mL) to obtain a final ANS concentration of 200 μM, and 20 μL of the mixed sample solution was dispensed into a 384-well black plate. Fluorescence spectra of ANS were recorded from 450 to 600 nm with an excitation wavelength of 385 nm at 25°C. The ANS fluorescence spectrum of each IgG1 sample was corrected by subtracting the spectrum of a blank solution of standard formulation MES buffer containing 200 μM ANS. For intrinsic fluorescence measurements, 20 μL of each IgG1 sample (3 mg/mL) was dispensed into a 384-well black plate. Intrinsic fluorescence spectra were recorded from 300 to 360 nm with an excitation wavelength of 285 nm at 25°C. The intrinsic fluorescence spectrum of each IgG1 sample was corrected by subtracting the spectrum of the blank solution of standard formulation MES buffer.

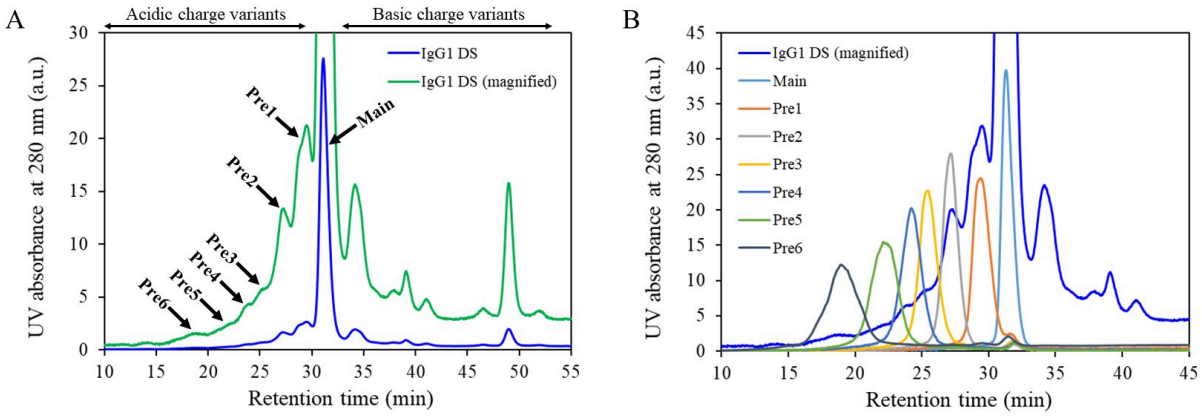

Fig. 1. (A) Representative CEX profile of the IgG1 drug substance (DS) used in this study. The acidic peaks investigated are designated *Pre1*, *Pre2*, *Pre3*, *Pre4*, *Pre5*, and *Pre6* in order of decreasing elution time. **(B)** CEX profiles of the *Main*, *Pre1*, *Pre2*, *Pre3*, *Pre4*, *Pre5*, and *Pre6* fractions isolated from the IgG1 DS. Magnified CEX profile of the IgG1 DS is shown as a reference.

3. Results

3.1 Purity check of isolated acidic and main fractions

A representative CEX profile of the IgG1 DS is shown in Figure 1A. A number of acidic/basic charge variants elute before/after the main peak (hereafter referred to as *Main*), which elutes at around 31 minutes. In this study, we focused on the physicochemical characterization of six acidic peaks, which, in order of decreasing elution time, are referred to here as *Pre1*, *Pre2*, *Pre3*, *Pre4*, *Pre5*, and *Pre6*, respectively. The *Main* and *Pre* fractions were isolated from the DS by preparative CEX, buffer-exchanged, and concentrated to over 3 mg/mL. These collected fractions were re-injected for analytical CEX to check the purity (Fig. 1B). The isolated *Main* fraction was found to be free of acidic and basic peaks. Each isolated *Pre* fraction still contained a small amount of *Main* peak, but was subjected to subsequent characterization without further purification.

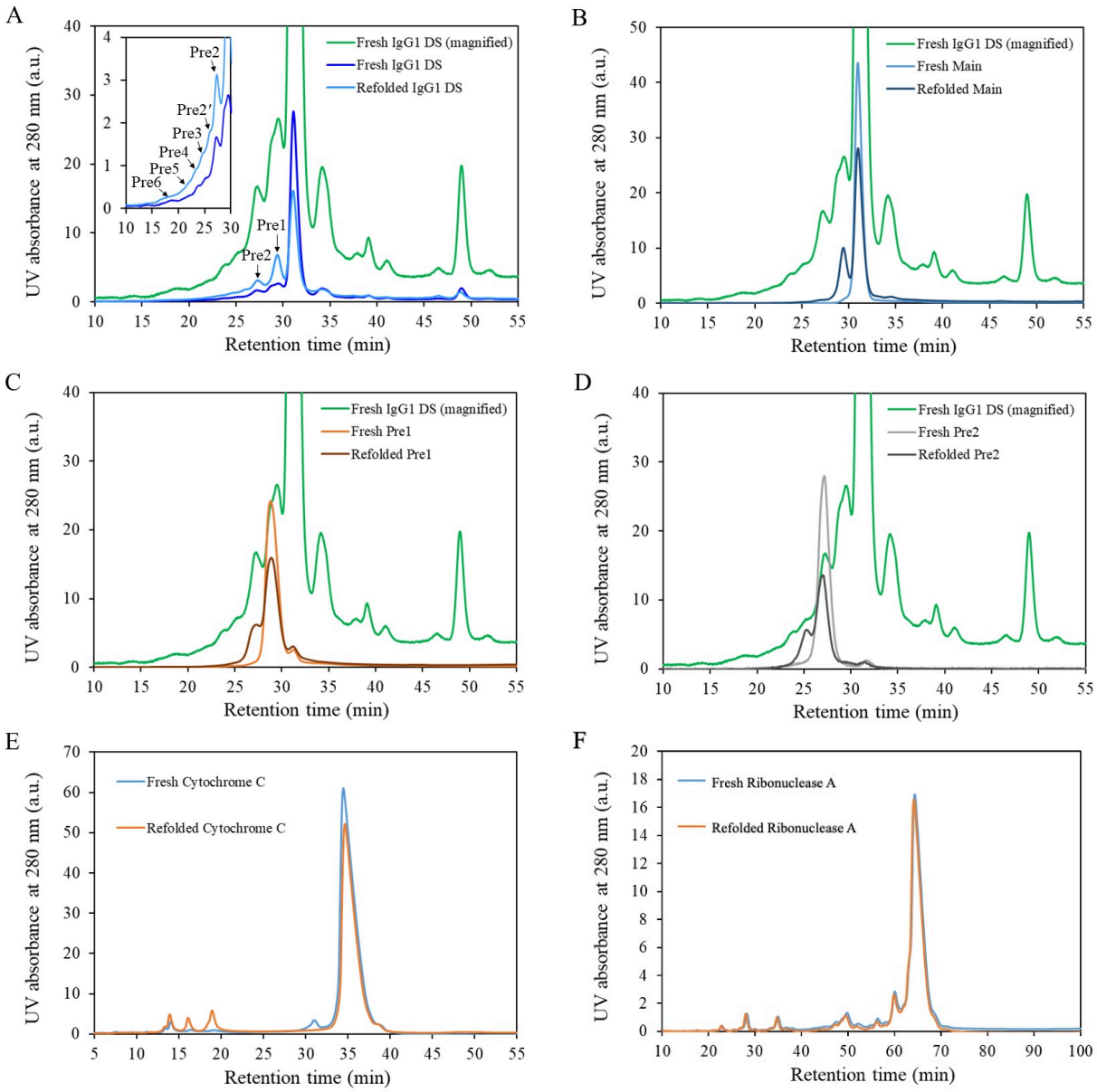

Fig. 3. CEX profiles of fresh (i.e., non-treated) and refolded **(A)** IgG1 drug substance (DS), **(B)** *Main*, **(C)** *Pre1*, **(D)** *Pre2*, **(E)** cytochrome C, and **(F)** ribonuclease A. The magnified CEX profile of the IgG1 DS is shown in **A**, **B**, **C**, and **D** as a reference. Inset in **A** depicts magnified elution profiles from 10 to 30 minutes. The refolding procedure is outlined in Figure 2.

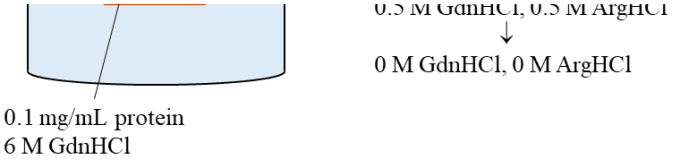

dialysis (GdnHCl: guanidine hydrochloride, ArgHCl: arginine hydrochloride).

To clarify whether the *Pre* peaks corresponded to conformational variants, we performed refolding experiments without a reducing agent. The IgG1 DS and isolated fractions were subjected to denaturation using 6 M guanidine hydrochloride, and were then refolded by stepwise dialysis as outlined in Figure 2. The concentration of guanidine hydrochloride was gradually reduced and 0.5 M arginine hydrochloride was utilized to suppress the formation of aggregates during the refolding process [23, 24]. The protein concentration was set as low as possible (i.e., 0.1 mg/mL) to avoid the formation of aggregates.

CEX profiles of fresh (i.e., non-treated) and refolded IgG1 DS are shown in Figure 3A. Following refolding, the area of the *Main* peak decreased, and that of each *Pre* peak increased. The longer the retention time of *Pre*, the greater the increase. A new peak that was not detected in the fresh IgG1 DS was

generated between the *Pre2* and *Pre3* peaks (depicted as *Pre2'* in Fig. 3A) after refolding. The total peak area of the samples was not changed during the refolding process (the ratio of refolded to fresh is 1.01), suggesting that almost no aggregates were generated under the refolding conditions. The isolated *Main* and *Pre* fractions were also each subjected to the refolding process to examine the changes in CEX profile. The CEX profiles of fresh and refolded *Main* fractions are shown in Figure 3B. The peak area of *Main* decreased, and *Pre1* and a small amount of *Pre2* were generated. *Pre1* generated from the *Main* fraction by the refolding process exhibited a symmetrical peak shape, whereas the *Pre1* peak in the fresh IgG1 DS was asymmetric, suggesting that the *Pre1* fraction contains multiple components with conformational variant being just one of them. Similarly, the isolated *Pre1* and *Pre2* fractions were refolded and analyzed by CEX (Fig. 3C and 3D). *Pre2* and *Pre3* peaks were generated from the *Pre1* and *Pre2* fractions, respectively. A *Main* peak was not generated from the *Pre1* and *Pre2* fractions.

To investigate whether the generation of acidic peaks by refolding is a general phenomenon that could occur in other proteins as well, we subjected cytochrome C and ribonuclease A to the same refolding process and CEX analysis (Fig. 3E and 3F). In cytochrome C, as in the IgG1 DS, the area of the main peak decreased, and the areas of the acidic peaks increased. An acidic peak eluting at around 31 minutes disappeared. In ribonuclease A, the CEX profile was not changed by the refolding process.

These results suggest that the acidic peaks in the IgG1 DS are conformational variants and that such variants could be generated in other proteins. To elucidate the conformational changes occurring in the *Pre* fractions, we characterized them using the following methods.

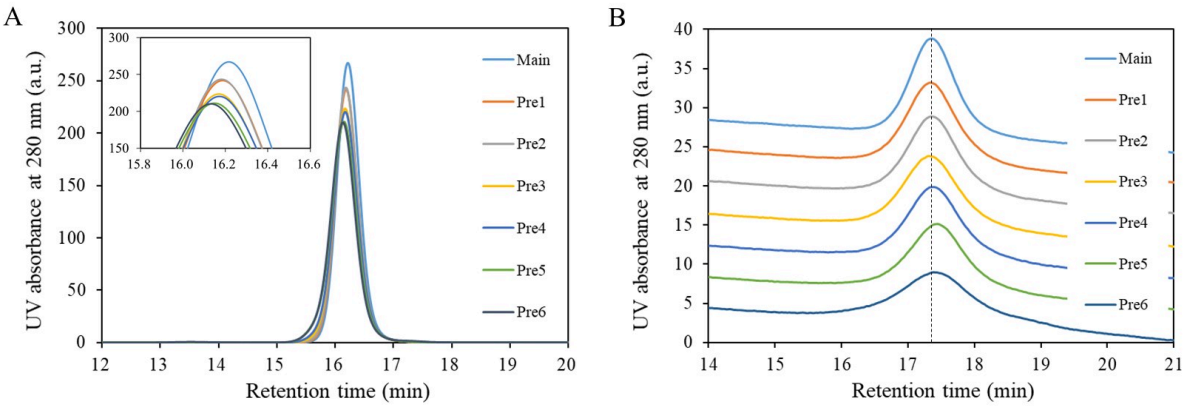

Fig. 4. **(A)** SEC and **(B)** HIC profiles of isolated *Main*, *Pre1*, *Pre2*, *Pre3*, *Pre4*, *Pre5*, and *Pre6* fractions. Inset in **A** depicts magnified elution profiles from 15.8 to 16.6 minutes. Dotted line in **B** shows the retention time of peak of *Main*.

3.3 SEC and HIC analysis

The isolated *Main* and *Pre* fractions were analyzed by SEC. All samples eluted as a single mAb monomer peak and no oligomers or aggregates such as dimers were detected (Fig. 4A). The shorter the elution time of *Pre* in CEX, the broader the monomer peak and the slightly shorter the elution time in SEC, suggesting that the conformational change of *Pre* variants altered their interaction with the SEC column resin or that the conformation of the *Pre* variants was slightly expanded compared to that of the *Main* variant. The isolated *Main* and *Pre* fractions were also analyzed by HIC (Fig. 4B). Similar to the SEC profiles, the shorter the elution time of *Pre* in CEX, the broader the peak in HIC. The retention times of *Pre4*, *Pre5*, and *Pre6* were slightly greater than that of *Main*, indicating that these *Pre* variants were slightly more hydrophobic than the *Main* variant.

Table 1 Hydrodynamic radius [R_h (nm)], radius of gyration [R_g (nm)], maximum dimension [D_{max} (nm)], and χ^2 of fit to the theoretical SAXS profile of isolated *Main*, *Pre1*, *Pre2*, *Pre3*, *Pre4*,

3.4 DLS and SAXS analysis

The R_h values of each fraction were determined by DLS measurements (Table 1). No difference in hydrodynamic properties were detected by DLS, and all samples showed the same R_h values (i.e., 5.3 nm), which is consistent with the R_h values reported for an IgG1 monomer [25]. SAXS profiles and the $p(r)$ functions of each fraction obtained at 20°C are displayed in Figure 5A and Figure 5B, respectively. The

[*a] obtained by DLS measurements at a concentration of 0.5 mg/mL at 25°C. Data represent the mean ± SD of three experiments.

[*b] obtained by SAXS measurements at a concentration of 1 mg/mL at 20°C.

[*c] obtained by fitting to the theoretical scattering profile from the crystal structure of a human IgG1 (pdb code:1hzh.pdb) with the ATSAS program CRYSOL [22].

SAXS profiles and $p(r)$ were typical of monomeric IgG1 [26] and no marked differences were detected between the *Main* and *Pre* fractions. The scattering profiles were compared to the theoretical scattering profile from the crystal structure of a human IgG1 (pdb code:1hzh.pdb) with the ATSAS program CRYSOL. The obtained χ^2 values are listed in Table 1 and range 1.3 to 1.6 suggesting a good agreement between the solution structure and model. The value of R_g and D_{max} were within the error estimates for different fractions (Table 1). These results suggest that the conformational changes occurring in the *Pre* variants are minor.

3.5 DSF analysis

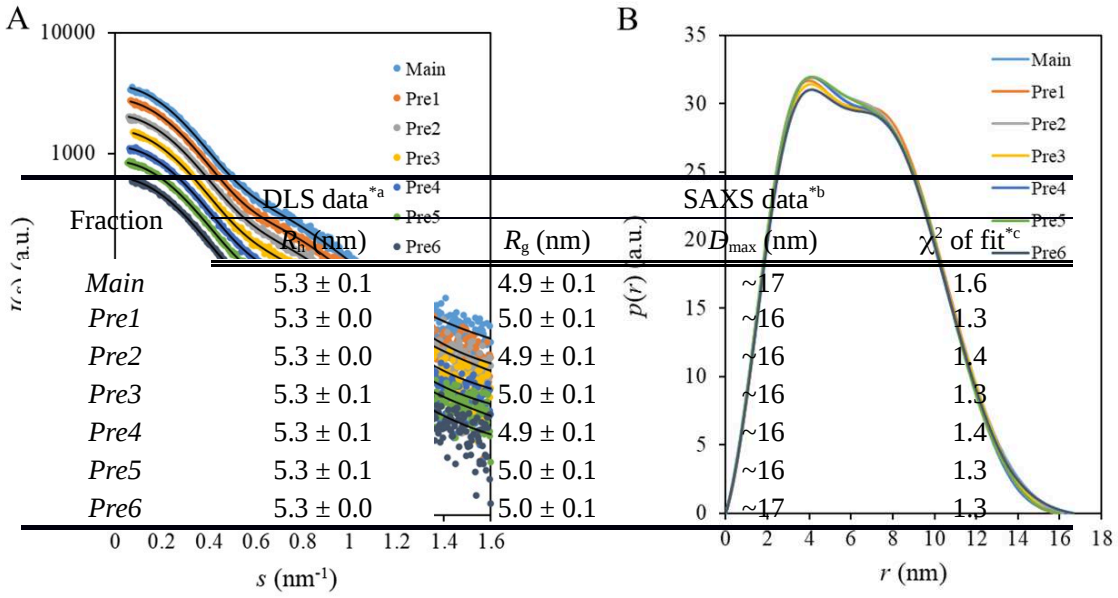

Fraction	DLS data*a R_h (nm)	R_g (nm)	SAXS data*b D_{max} (nm)	χ^2 of fit*c
Main	5.3 ± 0.1	4.9 ± 0.1	~17	1.6
Pre1	5.3 ± 0.0	5.0 ± 0.1	~16	1.3
Pre2	5.3 ± 0.0	4.9 ± 0.1	~16	1.4
Pre3	5.3 ± 0.1	5.0 ± 0.1	~16	1.3
Pre4	5.3 ± 0.1	4.9 ± 0.1	~16	1.4
Pre5	5.3 ± 0.1	5.0 ± 0.1	~16	1.3
Pre6	5.3 ± 0.0	5.0 ± 0.1	~17	1.3

Fig. 5. (A) SAXS profiles of isolated *Main*, *Pre1*, *Pre2*, *Pre3*, *Pre4*, *Pre5*, and *Pre6* fractions (1 mg/mL) at 20°C. The scattering data of *Pre* fractions were shifted downwards in logarithmic scale to avoid overlapping. Solid lines are the result of fitting by indirect Fourier transformation. **(B)** the pair–distance distribution function [$p(r)$].

For the IgG1 used in this study, thermal denaturation of the CH2, CH3, and Fab domains occurs separately in order of increasing temperature [27]. To clarify which domains potentially undergo conformational changes in the *Pre* variants, the T_m of each domain of the *Main* and *Pre* fractions was determined by DSF and compared. DSF thermograms of each fraction at pH 6.1 and pH 4.1 are shown in Figure 6A and Figure 6B, respectively. At pH 6.1, the T_m of the Fab domain exceeded the upper temperature limit of the instrument, and consequently the thermal denaturation of only the two domains of CH2 and CH3 could be detected; however, because the T_m of these domains decreases with the reduction in pH, the thermal denaturation of the three domains of CH2, CH3, and Fab could be detected at pH 4.1. The thermal denaturation curves almost overlapped between the samples, but slight differences between the *Main* and *Pre* fractions were detected in the CH2 and Fab domains. The T_m of the CH2 and CH3 domains at pH 6.1 are shown in Figure 6C and 6D, and the T_m of the CH2, CH3, and Fab domains at pH 4.1 are shown in Figure 6E, 6F, and 6G. The T_m of the CH2 domain of the *Pre* fractions was slightly lower than that of the

Main fraction at both pH values, but no marked difference was detected between the *Main* and *Pre* fractions in the CH3 domain. The T_m of Fab domain tended to be lower in the *Pre* fractions than in the *Main* fraction at pH 4.1, but the difference was extremely small. These results suggest that the conformational changes of the *Pre* variants are minor and occur at multiple sites, at least across the CH2 and Fab domains.

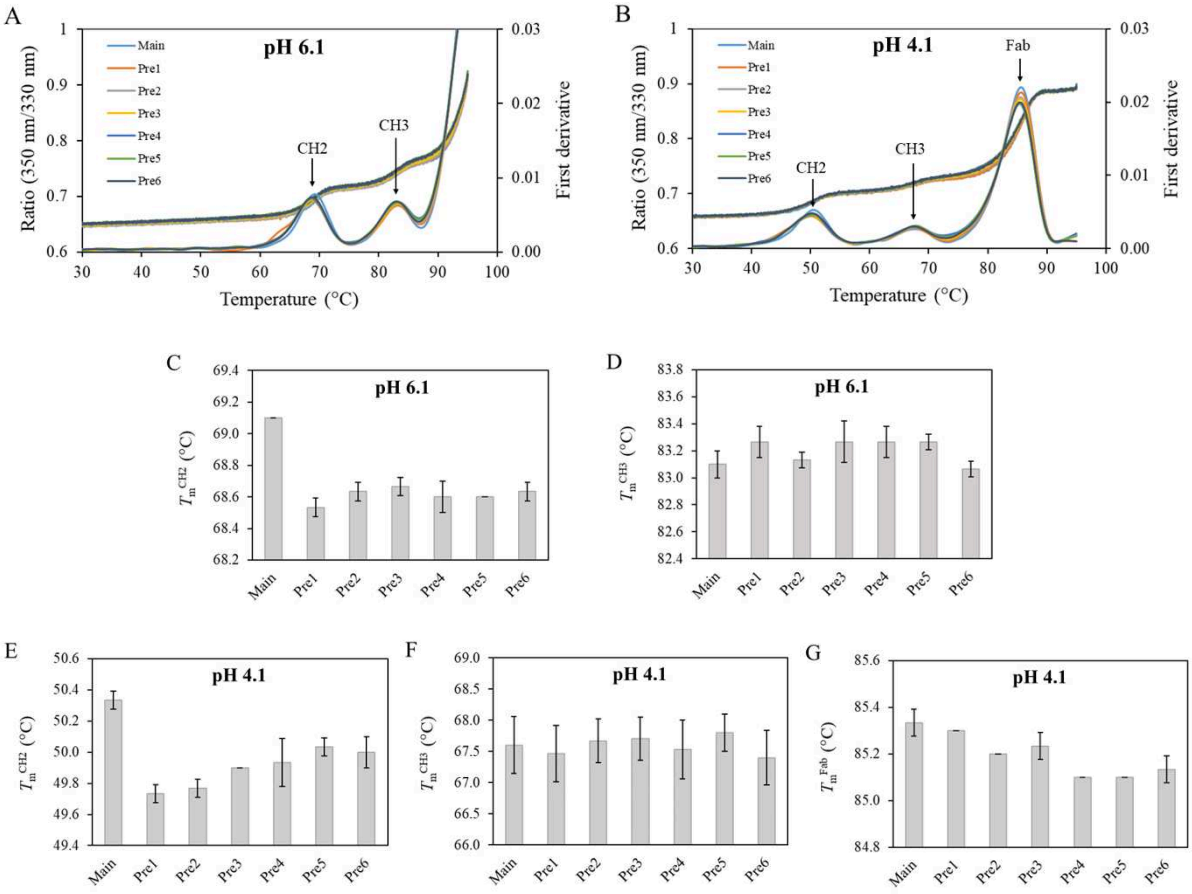

Fig. 6. DSF thermograms of isolated *Main*, *Pre1*, *Pre2*, *Pre3*, *Pre4*, *Pre5*, and *Pre6* fractions (0.5 mg/mL) at **(A)** pH 6.1 and **(B)** pH 4.1. The y-axes represent the ratio of intrinsic fluorescence at emission wavelengths of 330 and 350 nm (350 nm/330 nm) and the first derivative. Each curve represents the mean of three experiments. The peaks of the first derivative correspond to the thermal denaturation of CH2, CH3, and Fab domains in order of increasing temperature. The T_m (°C) of **(C)** CH2 and **(D)** CH3 domains at pH 6.1. The T_m of **(E)** CH2, **(F)** CH3, and **(G)** Fab domains at pH 4.1. Each column represents the mean ± SD of three experiments.

3.6 ANS and intrinsic fluorescence analysis

To further investigate the conformational changes occurring in the *Pre* variants, the hydrophobicity of each fraction was evaluated by ANS, a fluorescent probe that binds to hydrophobic regions. The ANS fluor

Fig. 7. **(A)** ANS fluorescence spectra of isolated *Main*, *Pre1*, *Pre2*, *Pre3*, *Pre4*, *Pre5*, and *Pre6* *Pre* fractions at 25°C. The concentrations of ANS and IgG1 were 200 μM and 2.7 mg/mL, respectively. The excitation wavelength was 385 nm. The fluorescence intensity was normalized to the intensity of the *Main* sample at 494 nm. Each curve represents the mean of three experiments. **(B)** Normalized fluorescence intensity at 494 nm and **(C)** λ_{max} (nm). Each column represents the mean ± SD of three experiments.

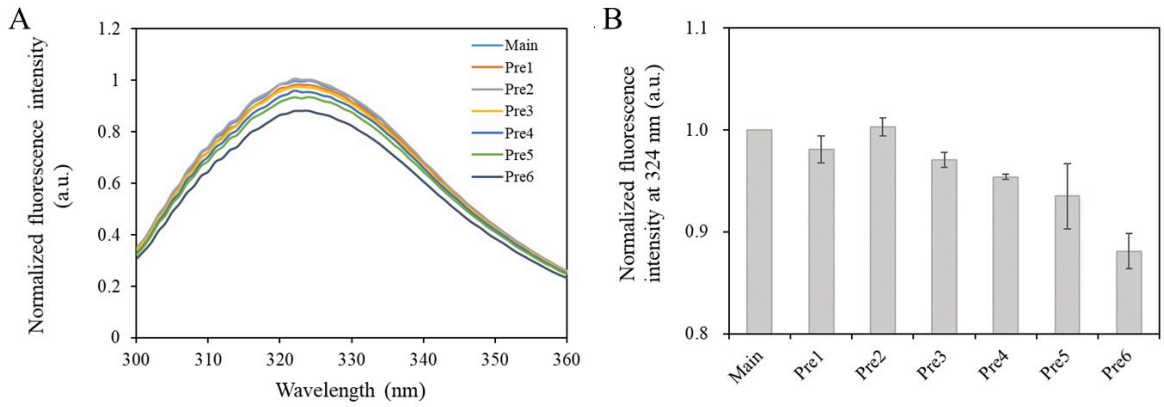

B

fractions at 25°C. The concentration of IgG1 was 3 mg/mL. The excitation wavelength was 285 nm. The fluorescence intensity was normalized by the maximum intensity of the *Main* sample. Each curve represents the mean of three experiments. **(B)** Normalized fluorescence intensity at 324 nm. Each column represents the mean ± SD of three experiments.

emission wavelength (λ_{max}) of ANS in the *Pre* fractions was slightly blue-shifted compared to that of the *Main* fraction. Subsequently, environmental changes around aromatic residues were investigated by intrinsic fluorescence measurements. The intrinsic fluorescence spectra under excitation at 285 nm are shown in Figure 8A. The fluorescence intensity tended to decrease slightly as the *Pre*-fraction number increased (Fig. 8B).

4. Discussion

As previous characterization studies on charge variants of therapeutic mAbs have shown, the full characterization of post-translational modifications in acidic variants of mAbs is challenging and remains an open area of investigation [9, 14–16]. It is usually found that quantitative measurements of identified acidic species leave some gaps, and that the sum of the identified acidic species does not fully account for the total acidic regions in the elution profile. Neill et al. reported that the basic variants of a mAb detected by CEX could be all fully accounted for by identified post-translational modifications, whereas the acidic variants could only be partially explained by deamidation and isomerization [9]. Dada et al. characterized both the acidic and basic regions of imaged capillary isoelectric focusing profile of an IgG1 mAb by using

preparative immobilized pH gradient isoelectric focusing fractionation and reported that unlike the basic variants where the detected modifications are discrete and exclusive, all acidic peaks to a varying degree shared similar modifications [16].

As described in Introduction section, the acidic fractions of the IgG1 mAb used in this study have also been extensively characterized previously by various techniques. However, interestingly, most of them showed no differences from the *Main* fraction (unpublished results). Since few post-translational modifications were detected, we speculated that the main attributes characterizing these unidentified acidic variants would be alterations in their higher order structure. Interestingly, Gervais et al. report that, on the basis of capillary isoelectric focusing, liquid chromatography-mass spectrometry, and liquid chromatography-tandem mass spectrometry data, the acidic variants of L-asparaginase do not include primary sequence modifications (such as deamidation), and they concluded on the basis of SAXS and ion mobility-mass spectrometry data showing slight conformational differences between the acidic and main peaks that the most prevalent acidic peak is a conformational variant [17]. That consideration was further supported by the results of refolding experiments demonstrating that the acidic peak could be converted into the main peak after unfolding using 8M urea and 2.2 M N-ethylurea and refolding by dialysis against water [17]. Even such a small conformational change may alter the overall surface charge distribution, owing to changes in the local distribution of charged residues. With reference to the study by Gervais et al., in this study we investigated whether conformational changes occur in the unidentified acidic variants of IgG1, and we analyzed the conformational changes occurring in the acidic fractions in more detail.

First, we examined whether refolding without a reducing agent could generate the acidic variants of IgG1. By applying stepwise dialysis, the use of arginine hydrochloride during refolding [23, 24], and a low concentration of the IgG1, we found conditions under which the IgG1 could be refolded without aggregation formation and under which the acidic variants could be generated. The results of the refolding studies revealed that the unidentified acidic variants of IgG1 would be conformational variants. Interestingly, *Pre1* was generated from *Main*, *Pre2* was generated from *Pre1*, and *Pre3* was generated from *Pre2* by the refolding process, suggesting that the acidity of the IgG1 molecular surface increased in a stepwise pattern as certain conformational changes accumulated in the *Main* molecule and these variants were eluted as multiple *Pre* peaks depending on the degree of accumulation of the conformational changes. The fact that only a small amount of *Pre2* and no *Pre3* were generated from *Main* is likely due to the low

probability of multiple conformational changes occurring simultaneously within a single molecule. With L-asparaginase, the refolding process generated the main peak from the acidic peak [17], but this was not the case for the IgG1 used in this study, presumably because the activation energy barrier for changing from *Pre* variants to the *Main* variant is very high in IgG1. The *Pre1* peak generated from *Main* by refolding process was symmetric. On the other hand, the *Pre1* peak originally contained in the IgG1 DS was asymmetric, which is likely due to the presence of sialylated IgG1 as described in Introduction section in addition to the conformational variant.

SAXS experiments were performed to investigate the conformational changes occurring in the *Pre* variants, but no marked differences in SAXS profiles were detected between the *Main* and *Pre* fractions, unlike in the case of L-asparaginase [17]. As well, no difference was detected between the *Main* and *Pre* fraction's R_h measured by DLS. These results indicate that the conformational changes occurring in the *Pre* variants are likely localized/minor and do not greatly affect the overall global disposition of the IgG1 in solution. Since IgG1 is a multi-domain/modular protein that is present in solution as a population-state ensemble, the minor conformational changes occurring in the *Pre* variants may be difficult to detect by SAXS due to the net averaging of conformational fluctuations. By isolating the Fc and Fab domains after fragmentation by enzyme treatment (such as papain digestion) and comparing the SAXS data between the *Main* and *Pre* fractions, it may be possible to identify those domains in which the conformational changes occur. However, isolating the Fc and Fab domains of the *Pre* fractions for SAXS experiments is time-consuming and labor-intensive; therefore, in this study, the SAXS experiments were limited to the measurement of the whole IgG1. Online CEX–SAXS, which can obtain SAXS data while isolating and purifying each domain using enzyme-treated IgG1, may be a suitable tool for detecting conformational changes occurring in the *Pre* variants [28–30]. Further studies will be required in order to detect the conformational changes in the *Pre* variants using SAXS.

In the SEC, HIC, DSF, and fluorescence analyses, slight differences were observed between the *Main* fraction and the *Pre* fractions, however, the differences detected were extremely small. The results of HIC and ANS fluorescence showed that the *Pre* variants were slightly more hydrophobic than the *Main* variant. In DSF, the T_m of the CH2 and Fab domains were slightly decreased in the *Pre* fractions, suggesting that the conformational changes in the *Pre* variants occur at multiple sites, at least across these two domains. The intrinsic fluorescence intensity of the *Pre* fractions decreased in a CEX retention time–dependent manner,

suggesting that the minor conformational changes of the *Pre* variants occur around aromatic residue regions. Wen et al. reported that microconformational changes within aromatic hydrophobic regions of several representative proteins could be induced by incubation with amine or guanidine additives [31]. Taking into account the results of that study, it could be assumed that, in the *Pre* variants, the side chains of aromatic residues are exposed to water due to local denaturation around the aromatic side chains, resulting in a decrease in the intrinsic fluorescence intensity and an increase in the hydrophobicity of the molecular surface. In SEC, the elution time of the monomer peak was slightly shorter for the *Pre* fractions; considering the results of HIC, fluorometry, and DSF, this was presumably due to the slightly expanded conformation of the *Pre* variants compared to that of the *Main* variant due to local denaturation. This hypothesis is consistent with the results of a previous study, in which SAXS measurements detected a slightly expanded state in the acidic peak of L-asparaginase [17].

For cytochrome C, acidic peaks were also generated by the refolding process. It is interesting to note that conformational variants resulting from the refolding process were detected as acidic peaks rather than basic peaks both in IgG1 and in cytochrome C. One possible explanation is that the exposure of aromatic amino acid side chains to water is induced by local denaturation, resulting in altered interactions with the column resin and the subsequent detection as acidic peaks. However, further studies are needed to clarify the mechanism of this phenomenon. On the other hand, refolding of ribonuclease A did not change the CEX profile, and no acidic peaks were generated. The stability of ribonuclease A is well known. The classical method for purification of ribonuclease A from bovine pancreas relies on its high stability that can maintain its integrity and solubility under severe conditions [32]. Conformational changes such as those seen in this study may be less likely to occur for highly stable proteins such as ribonuclease A.

5. Conclusion

Charge variation is one of the most common forms of heterogeneity in therapeutic mAbs, and thorough characterization of charge variants is important to identify critical quality attributes. However, it is not unusual that the sum of the quantitative values of the identified acidic species does not fully account for the total acidic regions in the elution profile. In this study, acidic variants of IgG1, which had been rarely identified in previous characterizations, were found to be generated by the process of refolding without a

reducing agent, indicating that these acidic variants are conformational variants. On the other hand, no conformational changes were detected by SAXS experiments for the intact IgG1, indicating that the conformational changes are minor. The results of HIC and ANS fluorescence showed that the *Pre* variants were slightly more hydrophobic than the *Main* variant. In DSF, the T_m of the CH2 and Fab domains were slightly decreased in the *Pre* fractions, suggesting that the minor conformational changes in the *Pre* variants occur at multiple sites, at least across these two domains. The intrinsic fluorescence intensity of the *Pre* fractions decreased in a CEX retention time–dependent manner, suggesting that the minor conformational changes of the *Pre* variants occur around aromatic residue regions. Taken together, these results suggest that, in the *Pre* variants, the side chains of aromatic residues are exposed to water due to local denaturation around the aromatic side chains, resulting in a decrease in the intrinsic fluorescence intensity and an increase in the hydrophobicity of the molecular surface. For cytochrome C, acidic peaks were also generated by the refolding process. One possible explanation is that the exposure of aromatic amino acid side chains to water is induced by local denaturation, resulting in altered interactions with the column resin and the subsequent detection as acidic peaks. Further studies are needed to elucidate in more detail the conformational changes, their formation mechanisms, and the mechanisms by which they are detected as acidic variants. This study provides new insights into the characterization of acidic variants of therapeutic mAbs that are not currently fully understood.

Acknowledgements

The authors thank Dr. Kohei Tsumoto (Medical Proteomics Laboratory, Institute of Medical Science, The University of Tokyo) for thoughtful discussions. The authors also thank Atsushi Watanabe, Yuka Funakoshi, So Yamaguchi, Akira Hayasaka, Chifumi Teramoto, and Kinue Shimizu for their support with experiments.

References

[1] H. Liu, G. Gaza-Bulseco, D. Faldu, C. Chumsae, J. Sun, Heterogeneity of monoclonal antibodies, J. Pharm. Sci. 97 (2008) 2426–2447.

[2] C.A. Boswell, D.B. Tesar, K. Mukhyala, F.P. Theil, P.J. Fielder, L.A. Khawli, Effects of charge on antibody tissue distribution and pharmacokinetics, Bioconjug. Chem. 21 (2010) 2153–2163.

[3] K.G. Moorhouse, W. Nashabeh, J. Deveney, N.S. Bjork, M.G. Mulkerrin, T. Ryskamp, Validation of an HPLC method for the analysis of the charge heterogeneity of the recombinant monoclonal antibody IDEC-C2B8 after papain digestion, J. Pharm. Biomed. Anal.

[4] M. Perkins, R. Theiler, S. Lunte, M. Jeschke, Determination of the origin of charge heterogeneity in a murine monoclonal antibody, Pharm. Res. 17 (2000) 1110–1117.

[5] R.J. Harris, B. Kabakoff, F.D. Macchi, F.J. Shen, M. Kwong, J.D. Andya, S.J. Shire, N. Bjork, K. Totpal, A.B. Chen, Identification of multiple sources of charge heterogeneity in a recombinant antibody, J. Chromatogr. B Biomed. Sci. Appl. 752 (2001) 233–245.

[6] S. Chung, J. Tian, Z. Tan, J. Chen, J. Lee, M. Borys, Z.J. Li, Industrial bioprocessing perspectives on managing therapeutic protein charge variant profiles, Biotechnol. Bioeng. 115 (2018) 1646–1665.

[7] J. Vlasak, R. Ionescu, Heterogeneity of monoclonal antibodies revealed by charge-sensitive methods, Curr. Pharm. Biotechnol. 9 (2008) 468–481.

[8] L.A. Khawli, S. Goswami, R. Hutchinson, Z.W. Kwong, J. Yang, X. Wang, Z. Yao, A. Sreedhara, T. Cano, D. Tesar, I. Nijem, D.E. Allison, P.Y. Wong, Y.H. Kao, C. Quan, A. Joshi, R.J. Harris, P. Motchnik, Charge variants in IgG1: Isolation, characterization, in vitro binding properties and pharmacokinetics in rats, MAbs. 2 (2010) 613–624.

[9] A. Neill, C. Nowak, R. Patel, G. Ponniah, N. Gonzalez, D. Miano, H. Liu, Characterization of recombinant monoclonal antibody charge variants using OFFGEL fractionation, weak anion exchange chromatography, and mass spectrometry, Anal. Chem. 87 (2015) 6204–6211.

[10] G. Ponniah, C. Nowak, A. Neill, H. Liu, Characterization of charge variants of a monoclonal antibody using weak anion exchange chromatography at subunit levels, Anal. Biochem. 520 (2017) 49–57.

[11] B. Yan, S. Steen, D. Hambly, J. Valliere-Douglass, T. Vanden Bos, S. Smallwood, Z. Yates, T. Arroll, Y. Han, H. Gadgil, R.F. Latypov, A. Wallace, A. Lim, G.R. Kleemann, W. Wang, A. Balland, Succinimide formation at Asn 55 in the complementarity determining region of a recombinant monoclonal antibody IgG1 heavy chain, J. Pharm. Sci. 98 (2009) 3509–3521.

[12] G.C. Chu, D. Chelius, G. Xiao, H.K. Khor, S. Coulibaly, P.V. Bondarenko, Accumulation of succinimide in a recombinant monoclonal antibody in mildly acidic buffers under elevated temperatures, Pharm. Res. 24 (2007) 1145–1156.

[13] X.C. Yu, K. Joe, Y. Zhang, A. Adriano, Y. Wang, H. Gazzano-Santoro, R.G. Keck, G. Deperalta, V. Ling, Accurate determination of succinimide degradation products using high fidelity trypsin digestion peptide map analysis, Anal. Chem. 83 (2011) 5912–5919.

[14] G. Ponniah, A. Kita, C. Nowak, A. Neill, Y. Kori, S. Rajendran, H. Liu, Characterization of the acidic species of a monoclonal antibody using weak cation exchange chromatography and LC-MS, Anal. Chem. 87 (2015) 9084–9092.

[15] Y.D. Liu, L. Cadang, K. Bol, X. Pan, K. Tschudi, M. Jazayri, J. Camperi, D. Michels, J. Stults, R.J. Harris, F. Yang, Challenges and strategies for a thorough characterization of antibody acidic charge variants, Bioengineering (Basel). 9 (2022) 641.

[16] O.O. Dada, N. Jaya, J. Valliere-Douglass, O. Salas-Solano, Characterization of acidic and basic variants of IgG1 therapeutic monoclonal antibodies based on non-denaturing IEF fractionation, Electrophoresis. 36 (2015) 2695–2702.

[17] D. Gervais, D. King, P. Kanda, N. Foote, L. Elliott, P. Brown, N.O. Lee, K. Thalassinos, C. Pizzey, R. Rambo, T.C. Minshull, M.J. Dickman, S. Smith, Structural characterisation of non-deamidated acidic variants of *Erwinia chrysanthemi* L-asparaginase using small-angle X-ray scattering and ion-mobility mass spectrometry, Pharm. Res. 32 (2015) 3636–3648.

[18] C.E. Blanchet, A. Spilotros, F. Schwemmer, M.A. Graewert, A. Kikhney, C.M. Jeffries, D. Franke, D. Mark, R. Zengerle, F. Cipriani, S. Fiedler, M. Roessle, D.I. Svergun, Versatile sample environments and automation for biological solution X-ray scattering experiments at the P12 beamline (PETRA III, DESY). J. Appl. Crystallogr. 48 (2015) 431–443.

[19] A. Round, F. Felisaz, L. Fodinger, A. Gobbo, J. Huet, C. Villard, C.E. Blanchet, P. Pernot, S. McSweeney, M. Roessle, D.I. Svergun, F. Cipriani, BioSAXS Sample Changer: a robotic sample changer for rapid and reliable high-throughput X-ray solution scattering experiments. Acta. Crystallogr. D Biol. Crystallogr. 71 (2015) 67–75.

[20] D. Franke, A.G. Kikhney, D.I. Svergun, Automated acquisition and analysis of small angle X-ray scattering data. Nucl. Inst. Meth. A. 689 (2012) 52–59.

[21] D.I. Svergun, Determination of the regularization parameter in indirect-transform methods using perceptual criteria. J. Appl. Crystallogr. 25 (1992) 495–503.

[22] D. Svergun, C. Barberato, M.H.J. Koch, CRYSOL–a program to evaluate X-ray solution scattering of biological macromolecules from atomic coordinates. J. Appl. Crystallogr. 28 (1995) 768–773.

[23] K. Tsumoto, K. Shinoki, H. Kondo, M. Uchikawa, T. Juji, I. Kumagai, Highly efficient recovery of functional single-chain Fv fragments from inclusion bodies overexpressed in *Escherichia coli* by controlled introduction of oxidizing reagent--application to a human single-chain Fv fragment. J. Immunol. Methods. 219 (1998) 119–129.

[24] M. Umetsu, K. Tsumoto, M. Hara, K. Ashish, S. Goda, T. Adschiri, I. Kumagai, How additives influence the refolding of immunoglobulin-folded proteins in a stepwise dialysis system. Spectroscopic evidence for highly efficient refolding of a single-chain Fv fragment. J. Biol. Chem. 278 (2003) 8979–8987.

[25] R. Bauer, A. Müller, M. Richter, K. Schneider, J. Frey, W. Engelhardt, Influence of heavy metal ions on antibodies and immune complexes investigated by dynamic light scattering and enzyme-linked immunosorbent assay. Biochim. Biophys. Acta. 1334 (1997) 98–108.

[26] W.G. Lilyestrom, S.J. Shire, T.M. Scherer, Influence of the cosolute environment on IgG solution structure analyzed by small-angle X-ray scattering. J. Phys. Chem. B. 116 (2012) 9611–9618.

[27] D. Kameoka, E. Masuzaki, T. Ueda, T. Imoto, Effect of buffer species on the unfolding and the aggregation of humanized IgG. J. Biochem. 142 (2007) 383–391.

[28] S. Hutin, M. Brennich, B. Maillot, A. Round, Online ion-exchange chromatography for small-angle X-ray scattering. Acta. Crystallogr. D Struct. Biol. 72 (2016) 1090–1099.

[29] M.E. Brennich, A.R. Round, S. Hutin, Online size-exclusion and ion-exchange chromatography on a SAXS beamline. J. Vis. Exp. 119 (2017) 54861.

[30] P.V. Konarev, M.A. Graewert, C.M. Jeffries, M. Fukuda, T.A. Cheremnykh, V.V. Volkov, D.I. Svergun, EFAMIX, a tool to decompose inline chromatography SAXS data from partially overlapping components. Protein Sci. 31 (2022) 269–282.

[31] L. Wen, M. Lyu, H. Xiao, H. Lan, Z. Zuo, Z. Yin, Protein aggregation and performance optimization based on microconformational changes of aromatic hydrophobic regions. Mol. Pharm. 15 (2018) 2257–2267.

[32] R.T. Raines, Ribonuclease A. Chem. Rev. 98 (1998) 1045–1066.